***RESEARCH ACCOMPLISHMENTS :***

After my initial training in computational chemistry, statistical mechanics and molecular spectroscopy, my postdoctoral research centered on the understanding of the structural and functional mechanisms of biological systems at the atomic level using computational approaches. My research has been interdisciplinary; bringing expertise in physical chemistry, quantum mechanics, chemical kinetics and statistical physics to important questions of structural biology.

In my first postdoctoral position with Dr. Carmay Lim (IBMS, Academia Sinica, Taipei, Taiwan) I developed an approach to study protein-ligand interactions and binding (Noskov 2001b). With a combination of methods, including molecular dynamics (MD) and continuum theories, it was possible to elucidate the determinants of the different binding affinities in the series of mutants of P53 core domain forming complexes with DNA (Noskov 2002; Wright 2002). This was the first study of P53-DNA complex with MD simulation in explicit solvent, and we combined these results with component analysis of free energies of binding. It helped to better understand molecular origins of human cancers since mutations in core domain of P53 protein are the major cause of lung cancer in human. In parallel, I was involved in research on the molecular origin of hydrophobic effects in binary water-alcohol mixtures at ambient and super-critical conditions using MD simulations (Kiselev 2001; Noskov 2001a). Throughout this period I carried out MD simulations for groups in the Academia Sinica and the Russian Academy of Sciences and I made major contribution to the development of free energy analysis algorithms at the IBMS, wrote many codes for supercomputers, gave many seminars for various departments and conferences, and assisted in the supervision of Ph.D. and undergraduate students at Russian Academy of Sciences.

To extend my training in biophysical theory I joined the group of Professor Benoît Roux at the Weill Medical College of Cornell University. My research at Cornell was focused on the analysis of the physical origin of ion selectivity in $K^+$ channels. Ionic selectivity is commonly explained in structural terms (see Figure 1 for structural model of selectivity filter in KcsA). However, there is a fundamental problem with this mechanism. Proteins are relatively flexible molecular structures, constantly undergoing thermal atomic fluctuations (~1.0 Å) while the difference in ionic radius between $K^+$ and $Na^+$ is very small (~0.4 Å). To address this issue, we have carried out molecular dynamics free energy perturbation simulations on the basis of the crystallographic structure of the KcsA embedded in a fully solvated lipid membrane. We found that the first coordination shell surrounding the ion in the narrow pore is very dynamical and "liquid-like" and that ion selectivity for $K^+$ does not arise from the precise sub-angstrom geometry and the architectural rigidity of the narrow pore as commonly assumed. The analysis demonstrates that ion selectivity is a robust feature of such a flexible pore symmetrically line by fluctuating backbone carbonyl groups (Noskov 2004a). Results of this work significantly changed the conventional view of ion selectivity and provided a physical approach for a future drug development. However, the understanding of chemistry behind fast conduction and selectivity is still a future goal. To further elucidate the role of hydration in the dynamics and energetic of $K^+$ in the cavity of KcsA channel I initiated *QM/MM* simulations in Dr. Roux's group.

I have participated in the development of the program code for Grand Canonical Monte-Carlo/Brownian Dynamics simulations with inclusion of a method to treat of non-uniform ion diffusion in the pore. My calculations on the *α-hemolysin* toxin provided a structural explanation to an important physiological function, namely weak anion selectivity and asymmetric conduction (Noskov 2004b). We started the development of polarizable potential functions for proteins. Using combination of quantum mechanics with molecular dynamics simulations to create a polarizable potential function for ethanol (threonine side-chain mimetic), we have obtained better agreement with experiment (dielectric constant, diffusion and thermodynamic properties) than ever before (Noskov 2004c). Furthermore, these studies explained unexpected results of neutron-diffraction scattering and significantly changed the traditional view of the hydrophobic effect. Our developments of improved computational methods for studying proteins have opened the door for the future research where computer simulations can be used to understand the mechanisms responsible for many problems of chemical, biological and medical significance.

***PROPOSED RESEARCH PROJECT:***

***BACKGROUND AND SIGNIFICANCE:*** Biological channels are comprised of bilayer-spanning proteins that catalyze the movement of ions and molecules through phospholipid bilayer. Ever since the early days of electrophysiology and biophysics, theoretical models have contributed to a better understanding of the channels functions. In a last few decades a very robust theoretical and computational framework was developed for studies of ion passage through different pores (Roux 2004). Recently, computational studies revealed the physical mechanisms of ion conduction and selectivity in $K^+$ channels(Berneche 2003; Noskov 2004a). Although, the physics of the conduction and selectivity was studied in great detail, many important questions remain unclear: the interplay between multi-ion states and hydration of ions in different binding sites as well as channel selectivity; the role of induced polarization in ion transport and many others. Further studies using methodologies previously developed may highlight chemical origins of ion selectivity and fast conductance in $K^+$ channels. An important problem in the field, which has been hardly studied by molecular modeling, is transport and binding of small organic molecules. For example, the emergence of bacterial multidrug resistance is an increasing problem in the treatment of infectious diseases (Zgurskaya 1999). Experimental studies provided ample information regarding structures and functions of biological pores (Murakami 2002; Pos 2004) but theoretical considerations are necessary to elucidate macroscopic factors governing channel functions.

Recent genome sequence analysis indicated that bacteria have a large number of putative drug exporter genes. They are subdivided into 5 families: major facilitator superfamily (MSF), small multidrug resistance (SMR), resistance nodulation division (RND), multidrug and toxic compound extrusion (MATE) and ATP-binding cassette (ABC). The first 3 classes comprise in the largest bacterial family of tetracycline/$H^+$ antiporters, MATE is a $Na^+$/drug antiporter and ABC is group of transporters activated by ATP hydrolysis. The success in structural characterization of RND-type drug exporters such as AcrB and MexB transporters opens the door for future theoretical studies.

AcrB is the active part of the AcrAB-TolC drug export complex(Murakami 2003). The transmembrane domain (TM) of each protomer of AcrB is composed of 12 $\alpha$ helices(Murakami 2002) (See Figure 2). The striking feature of the AcrB trimer is the presence of the three vestibules open to the periplasm. Substrates can access to the central cavity from the periplasmic surface and then be actively transported through the pore. Yu et al. (Yu 2003) used electron density-omit maps to identify drug-binding sites. Because specific interactions rely on the three-dimensional protein (and drug) structure, it becomes important to understand of the energetic of drug transport. The combination of high-resolution crystal structures of RND proteins(Pos 2004) with highly sophisticated computational approaches offers us a possibility to link channel structure to its functions.

It is important, however, to focus first on model systems that will allow to test methodologies, provide insight, and permit quantitative comparison with experiment such as OmpF porin or KcsA/KirB channels. I already started simulation studies of $K^+$ channels function and some of the techniques we used can be transferred to the problems discussed above. The current framework, based on Mori-Zwanzig projection operator formalism, can be extended for studies of antibiotics translocation(Roux 2004). Within this framework, the fundamental ingredients such as PMF (potential mean force) and memory functions will be calculated using all-atom MD simulations. To reduce the conformational space sampled for PMF computations, only position of the center of mass of the ligand will be used in combination with steered MD to insure location in the channel. It will allow us to average different conformations of the ligand inside the pore as well will guide the future BD simulation with an effective PMF profile. The general diffusion porin OmpF (Cowan 1992) (outer membrane protein F) is considered to be the primary gateway for antibiotics (Nestorovich 2002) crossing outer membrane and then transported by the AcrAB complex (Murakami 2003). This system can be used to calibrate protocols for studies of antibiotics with different functional groups. An experimental information from the group of Dr. S.M. Bezrukov *(NICHD,NIH)* will provide the guidance in parameter developments and calibration. Additional test ground of high physiological importance may be supplied by the family of $K^+$ channels. Potassium channels were rigorously studied over the last decade both structurally (Doyle 1998, Kuo 2003) and functionally (Lopatin 1994, Nichols, 1997). They are a good probe for the testing of algorithm and the initial theoretical studies of organic molecule binding. Structures and the functions of these channels are well characterized experimentally; they are amenable to computer simulations, and their transport properties are sensitive to point mutations, which alter the size of the pore region.

My major goal is the microscopic understanding of the regulation of drug trafficking through protein complexes. Special attention will be paid to the chemical mechanism behind proton transfer and drug translocation in AcrB transporter. This process is initiated by the binding of different substrates to the central cavity of AcrB (Yu 2003). The latter is believed to be the origin of extraordinarily broad substrate specificity. It is known that protonation of Asp408/Asp407-Lys940 triad located at the entrance to the TM domain of AcrB plays an important role for tetracycline transport (Murakami, 2003). Questions about the microscopic factors determining proton dynamics in AcrB system may be addressed using combined QM/MM molecular dynamics (Hayashi 2003; Rousseau 2004). It will be complimented by detailed MD studies of antibiotics binding and PMF profiles of drug transport through AcrB transmembrane domain. Most of the existing force-fields typically account for many-body polarization effects using effective approximation of the atomic partial charges. Such potential functions can lead to meaningful results, but an effective potential function may not be consistently reliable, under all conditions relevant to biomolecules.

***SPECIFIC AIMS:***

1. Thermodynamics of substrate-binding affinity in transporter trans-membrane domain (long-standing goals):
   - MD simulations of protonated and deprotonated forms of AcrB to elucidate principal differences in dynamics.
   - QM/MM studies of proton transfer via *Asp408/Asp407-Lys940* ion pairs.
   - Simulations of ligand binding to the central cavity of AcrB to reveal origins of specificity.
2. Dynamics and energetic of transport through biological pores (short-term goals).
   - PMF computations for polyamines binding to the KcsA/KirB channels.
   - MD simulations to obtain PMF profiles for antibiotic transport through OmpF. *(Dr. S.M. Bezrukov (NIH) is willing to provide an experimental guidance for these studies).*
   - BD simulations of the antibiotic transport using PMF profiles from MD simulations for OmpF and TM of AcrB.
3. Methodological development of simulation techniques.
   - Developing of BD simulation technique for multi-site objects transport guided by PMF functions from MD.
   - Elucidation of the effect of induced polarization onto dynamics in biological channels.
   - Participation in the development of first generation of all-atom polarizable potential functions on the base of atomic point charges and the classical Drude oscillator model. *(In collaboration with Benoît Roux (Cornell) and Alex D. MacKerell (U. Maryland)).*

***RESEARCH PLAN AND METHODS:*** It is known that studies of proton dynamics in biological systems are incomplete without accounting for quantum effects. Quantum-mechanical and mixed QM/MM simulation techniques may be employed to calculate proton transfer pathways in AcrB system. Aimed initially at the simulation of enzymatic reactions, the QM/MM approach consists in partitioning the protein into two subsystems, so as to treat the portion directly involved in the chemical reaction at the QM level (the QM subsystem), whereas the remainder, where events such as bond breaking and bond formation do not take place, is represented by a MM force field. Despite its obvious usefulness, the main limitation in the use of QM/MM simulation is a relatively short time-scale of simulations. To complement QM/MM studies, classical simulations and MD modeling with polarizable force-fields (Lamoureux 2003; Noskov 2004c) of protonated and deprotonated forms of AcrB TM domain will be performed. Our preliminary efforts toward the development of a polarizable force-field for CHARMM have concentrated on the parameterization of essential functional groups (gas-phase properties, solvation energies, dielectric, thermodynamic and transport characteristics in a condensed phase). This work will be continued and polarizable potential function will be applied for MD simulations of biomolecules.

A useful approach to study antibiotic dynamics in a confined environment is steered, (or targeted MD), where the ligand position along the pore is enforced by application of a force, whereas the positions of atoms in the exterior of the pore are restrained. Because studies of drug transport properties may require a microsecond simulation, methods that permit extension into large time-scales will be used. This may be achieved by connecting properties of the microscopic system to a macroscopic by use of stochastic trajectories from Brownian dynamics. It was in this fashion then I studied ion transport in *α-hemolysin* system.

**Energetic of the ligand partitioning in biological pores:** The thermodynamics of binding of small organic compounds and ions into will be studied using the following approach. To start, I will perform PMF computations for different multi-ion states in the well-characterized KcsA channel. To characterize the possible mode of polyamines binding in KcsA and

KirB channels, MD simulations with docked ligands will be used. By elucidating the principal energetical barriers and modes of polyamine binding in the confined environment of the channel we will understand the chemical basis of the conjunction between high conductance rates and ion selectivity in narrow pores. In addition to its great physiological importance, this work will help us to calibrate our methods to be applied for studies of ion (some divalent ions and protons) and small organic molecule dynamics in transporters. Once these important benchmarks have been set, MD simulations of antibiotics bound to the cavity of AcrB will be considered (Yu 2003). I will calculate the free energy of binding ($\Delta G$), principal components and per-residue contributions for 4 different antibiotics: rhodamine, ethidium, dequilinium and ciprofloxacin. These calculations will provide a molecular basis of multiple drug-binding capacity of the AcrB multidrug efflux pump. Importantly, the microscopic interactions of different amino-acid residues with antibiotics will be revealed, which experiment is not able to provide.

**Transport of antibiotics through the biological pores:** Non-equilibrium Brownian dynamics (Ermak 1978) of the multi-site model compound(Allison 1991; Beard 2003) in a simple hydrophobic cylinder will be considered. It is possible to determine the potential between wall and multi-side particle as well as membrane potential from the solution of the linearized Poisson-Boltzmann equation in the same fashion as we did for simulation of ion flow through $\alpha$-hemolysin(Noskov 2004b). Then I will study then dynamics of different antibiotics in the outer membrane protein (OmpF). To obtain a clear understanding of ligand influence on the local conformational dynamics in proteins, I will perform PMF computations of the ligand transport through OmpF porin using steered MD simulations. This set of PMF will guide the study of antibiotic transport using Brownian Dynamics.

**Modulation of antibiotic transport in AcrB transporter:** The culmination of this work will be a *QM/MM* simulation of proton transport in *Asp408/Asp407-Lys940* triad. (See Figure 2). Site-directed mutagenesis studies indicated that these residues are essential for a drug transport and functions of AcrB. It is believed that the driving force for AcrB-mediated drug transport is the proton motive force. Proton capture and release are hypothesized to be the source of different substrate-binding affinities due to small conformational changes, which lead to close/open forms of the TM domain. QM and QM/MM simulations can help to determine energetic of the proton translocation in the ionic triad. The structures obtained by QM/MM and classical MD simulations will be used to perform BD studies of tetracycline transport in two different forms of AcrB TM domain. It is possible to build a series of models to mimic different open/close conformations of AcrB and perform BD simulations to probe the opening dynamic. My hope is that this knowledge will aid our understanding of molecular mechanisms of multi-drug export and proton-coupled transport in bacterial proteins.

***SUMMARY:*** With current access to inexpensive computational resources, theoretical methods can be used to infer equilibrium and dynamical properties of biological systems and link microscopic mechanisms to the available structural and functional information. The ultimate scientific goal of the proposed research is to identify the fundamental principles that govern transport of organic molecules in biological pores. This will be accomplished by using a multilevel, comparative, and hierarchical approach (BD$\rightarrow$ MD $\rightarrow$ MD with polarizable potential function $\rightarrow$ *QM/MM* simulations). By explaining how molecular structure determines binding and transport of antibiotics to the cell, we will aid future experimental research and design of new efficient medical agents.

***TEACHING STATEMENT:*** I want to participate in undergraduate and graduate education in computational biochemistry/biophysics, statistical mechanics and bioinformatics, through the development and teaching of courses, research seminars, and tutoring of undergraduate and graduate research assistants. On a longer term, I would like to help establish undergraduate and graduate specializations in computational biology, with special emphasis on rigorous statistical and quantum-mechanical methods. As a byproduct of these initiatives, I would like to help in the shaping of the undergraduate and graduate curriculum, to bring an interdisciplinary approach into teaching by connecting physics and chemistry to biological processes. My motivation is that further development of computational chemistry and biology methods may require from students a good understanding of both conceptual and practical aspects. Relevant courses would include: computational biology, quantum chemistry, statistical mechanics and molecular modeling.

**Cited Literature:**

Allison SA. 1991. A Brownian dynamics algorithm for arbitrary rigid bodies. Applications to polarized dynamic light scattering. ***Macromolecules*** **24**:530-536.

Beard DA, Schlick, T. 2003. Unbiased rotational moves for rigid body dynamics. *Biophys.J.* **85**:2973-2976.

Berneche S, Roux, B. 2003. A Microscopic View of Ion Conduction Through the KcsA K+ Channel. *Proc.Natl.Acad.Sci. USA* **100**:3025-3039.

Cowan S, Schrimmer, T., Rummel, G., Steiert, M., Ghosh, R., Pauptit, R. et al. 1992. Crystal structures explain functional properties of two E.coli. porins. *Nature* **358**(243):727-733.
Doyle DA, Cabral, J.M., Pfuetzner, R.A., Kuo, A., Gulbis, J.M., Cohen, S.L., Chait, B.T., MacKinnon, R. 1998. The structure of the potassium channel: molecular basis of K+ conductance and selectivity. *Science* **280**:69-77.
Ermak DL, McCammon, J.A. 1978. Brownian Dynamics with Hydrodynami Interactions. *J.Chem.Phys.* **69**:1352-1360.
Hayashi S, Tajkhorshid, E., Shulten, K. 2003. Molecular Dynamics Simulation of Bacteriorhodopsin's Photoisomerization using *ab-initio* Forces for the Excited Chromophore. *Biophys. J.* **85:**1440-1449.
Kiselev MG, Noskov, S.Y., Puhovski, Y.P., Kerdcharoen, T., Hannongbua, S. 2001. Study of hydrophobic hydration in super-critical methanol-water mixtures. *J. Mol. Graph. Model.* **19:**412-416.
Kuo A, Gulbis, J.M., Antcliff, J.F., Rahman, T., Lowe, E.D., Zimmer, J., Cuthbertson, J., Ashcroft, F.M., Ezaki, T., Doyle, D.A. 2003. Crystal structure of the potassium channel KirBac1.1 in the closed state. *Science* **300**:1922-1926.
Lamoureux G, MacKerell, A.D., Roux.B. 2003. A Simple Polarizable Model of Water Based on Classical Drude Oscillators. ***J.Chem.Phys.*** **119**:5185-5197.
Lopatin AN, Makhina, E.N., Nichols, C.G. 1994. Potassium channel block by cytoplasmic polyamines as the mechanism of intrinsic rectification. *Nature* **372:**366-369.
Murakami S, Nakashima, R., Yamashita, E., Yamaguchi, A. 2002. Crystall structure of bacterial multidrug efflux transporter AcrB. *Nature* **419**:587-593.
Murakami S, Yamaguchi, A. 2003. Multidrug-exproting secondary transporters. *Current Opinion in Structural Biology* **13**(443-452).
Nestorovich EM, Danelon, C., Winterhalter, M., Bezrukov, S.M. 2002. Designed to penetrate:Time-resolved interaction of single antibiotic molecules with bacterial pore. *Proc.Natl.Acad.Sci. USA* **99**:9789-9794.
Nichols C, Lopatin, A. 1997. Inward rectifier potasium channels. *Annu.Rev.Physiol.* **59**:171-191.
Noskov SY, Berneche.S., Roux, B. 2004a. Control of ion selectivity in potassium channels by electrostatic and dynamic properties of coordinating ligands. *Nature* in press.
Noskov SY, Im.W., Roux, B. 2004b. Permeation through the alpha-hemolysin Channel: Theoretical Studies Based on Brownian Dynamics and Poisson-Nernst-Plank Electrodiffusion Theory. *Biophys.J.* **87**(3).
Noskov SY, Kiselev, M.G., Rode, B.M., Kolker, A.M. 2001a. Structure of methanol-methanol associates at dilute methanol-water mixtures from molecular dynamics simulation. *J.Mol.Liq.* **91**:157-165.
Noskov SY, Lamoureux, G., Roux, B. 2004c. Microscopic picture of hydrophobic hydration in water-ethanol mixtures from simulation with new polarizable force-field. J.Am.Chem.Soc. submitted.
Noskov SY, Lim, C. 2001b. Free energy decomposition of protein-protein interaction. *Biophys.J.*, **81**:737-750.
Noskov SY, Wright, J.D., Lim, C. 2002. Long-Range Effects of Mutating R248 to Q/W in the p53 Core Domain. *J.Phys.Chem.B* **106**:13047-13057.
Pos KM, Schiefner, A., Seeger, M.A., Diederichs, K. 2004. Crystallographic analysis of AcrB. *FEBS Lett.* **564:**333-339.
Rousseau R, Kleinschmidt ,V, Schmitt, UW, Marx, D. 2004. Modeling protonated water networks in bacteriorhodopsin. *Phys.Chem.Chem.Phys.* **6**:1848-1859.
Roux B, Allen, T., Berneche, S., Im.W. 2004. Theoretical and computational models of biological ion channels. *Quart.Rev. Biophys.* **37**:15-103.
Wright JD, Noskov, S.Y., Lim.C. 2002. Factors governing loss and rescue of DNA binding upon single and double mutations at P53 core domain. *Nucl.Acids.Res.* **30**:1563-1574.
Yu E, McDermott, G., Zgurskaya, H.I., Nikaido, H., Koshland, D.E., Jr. 2003. Structural basis of multiple drug-binding capacity of the AcrB multidrug efflux pump. *Science* **300**:976-980.
Zgurskaya HI, Nikaido, H. 1999. Bypassing the periplasm: Reconstitution of the AcrAB multidrug efflux pump of Escherichia coli. *Proc.Natl.Acad.Sci. USA* **96:**7190-7195.

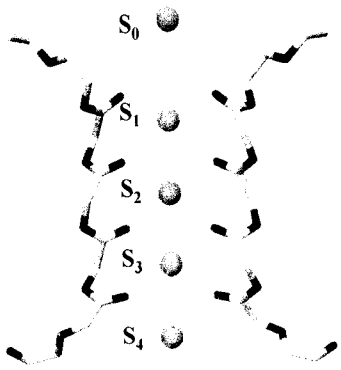


**Figure 1.** Schematic structure of the cation binding sites in the selectivity filter of the KcsA channel. Only two subunits are depicted for clarity. The extracellular side is on the top and the intracellular side is at the bottom. Results from both x-ray crystallography and molecular dynamics (MD) free energy simulations show that five specific cation binding sites ($S_0$ to $S_4$) are disposed along the narrow pore of the KcsA $K^+$ channel. The cations are represented (green) and the carbonyl oxygen group of residues Thr75, Val76, Gly77 and Tyr78 are shown explicitly (red).

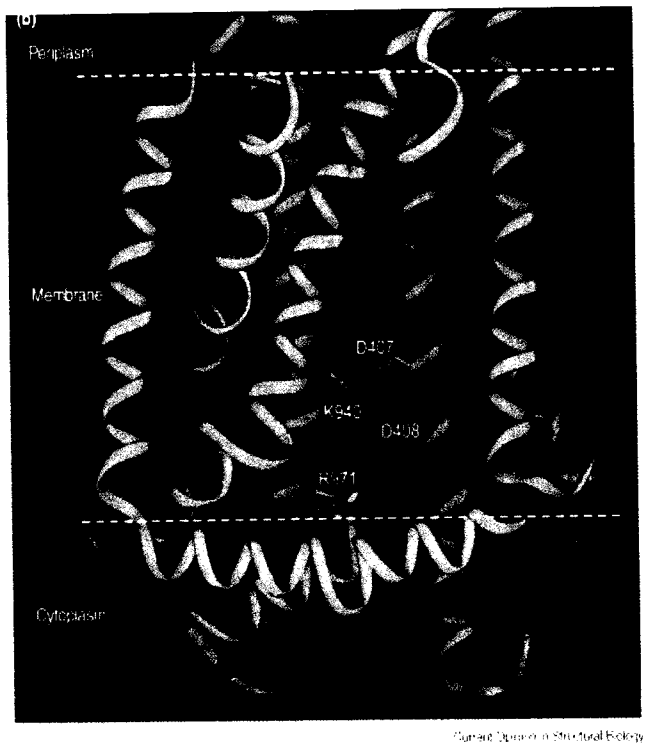


**Figure 2.** Side view of the transmembrane region of AcrB. Sidechains of essential charged residues are depicted. The broken arrow indicates the proposed proton translocation pathway (Murakami,2002).

# List of Scientific Referents of Dr. Sergei Noskov (Weill Medical College of Cornell University).

1. Professor **Benoît Roux**
Head of Computational Biology Group;
Department of Biochemistry, Department of Physiology and Biophysics;
Weill Medical College of Cornell University
1300 York Avenue, New York, NY 10021
Phone: 212-746-6018
Fax: 212-746-4843
E-mail: ber2004@med.cornell.edu; benoit.roux@med.cornell.edu

2. Professor **Carmay Lim**
Head of Computational Biophysics Program
Department of Structural Biology
Institute of Biomedical Sciences,
Academia Sinica, Taipei 11529, Taiwan
Phone: +011-886-2-2652-3031
Fax : +011-886-2-2788-7641
E-mail: carmay@gate.sinica.edu.tw

3. Professor, Dr.Sci. **Michael Kiselev**
Head of Theoretical Department
Institute of Solution Chemistry, Russian Academy of Sciences
Akademicheskaya street, 1, 153045, Ivanovo, Russia
Phone: +011-7-0932-351869
Fax: +011-7-0932-378509
E-mail: mgk@isc-ras.ru

4. Assistant Professor **Toby W. Allen**
Computational Chemistry and Biophysics
University California at Davis
One Shields Avenue • Davis, CA 95616
Phone: 530-754-5968
e-mail: twallen@ucdavis.edu

5. Professor **Olaf S. Andersen** ;

Professor of Physiology,
Director, Program in Physiology, Biophysics and Molecular Medicine
Cornell Graduate School of Medical Sciences
1300 York Avenue New York, NY 10021
Phone:212-746-6350
e-mail: sparre@med.cornell.edu

# Ion Permeation through the α-Hemolysin Channel: Theoretical Studies Based on Brownian Dynamics and Poisson-Nernst-Plank Electrodiffusion Theory

Sergei Yu. Noskov,* Wonpil Im,† and Benoît Roux*

*Department of Biochemistry & Structural Biology, Weill Medical College of Cornell University, New York, New York 10021; and †Department of Molecular Biology (TPC6), The Scripps Research Institute, La Jolla, California 92037

ABSTRACT Identification of the molecular interaction governing ion conduction through biological pores is one of the most important goals of modern electrophysiology. Grand canonical Monte Carlo Brownian dynamics (GCMC/BD) and three-dimensional Poisson-Nernst-Plank (3d-PNP) electrodiffusion algorithms offer powerful and general approaches to study of ion permeation through wide molecular pores. A detailed analysis of ion flows through the staphylococcal α-hemolysin channel based on series of simulations at different concentrations and transmembrane potentials is presented. The position-dependent diffusion coefficient is approximated on the basis of a hydrodynamic model. The channel conductance calculated by GCMC/BD is ~10% higher than (electrophysiologically measured) experimental values, whereas results from 3d-PNP are always 30–50% larger. Both methods are able to capture all important electrostatic interactions in equilibrium conditions. The asymmetric conductance upon the polarity of the transmembrane potential observed experimentally is reproduced by GCMC/BD and 3d-PNP. The separation of geometrical and energetic influence of the channel on ion conduction reveals that such asymmetries arise from the permanent charge distribution inside the pore. The major determinant of the asymmetry is unbalanced charge in the triad of polar residues D127, D128, and K131. The GCMC/BD or 3d-PNP calculations reproduce also experimental reversal potentials and permeability rations in asymmetric ionic solutions. The weak anionic selectivity of the channel results from the presence of the salt bridge between E111 and K147 in the constriction zone. The calculations also reproduce the experimentally derived dependence of the reversible potential to the direction of the salt gradient. The origin of such effect arises from the asymmetrical distribution of energetic barriers along the channel axis, which modulates the preferential ion passage in different directions.

## INTRODUCTION

Staphylococcal α-hemolysin (α-HL) is a toxin protein involved in a number of human diseases. Available experimental studies show that this toxin is a major determinant of a bacterial pathogenicity for *Staphylococcus aureus* (Bhakdi and Tranum-Jensen, 1991; Alouf and Freer, 1999), which causes different urinary tract infections (Gentschev et al., 2002) and pyelonephritis (Laestadius et al., 2002). It is also known that the toxin is an important virulence factor due to its cytolytic and cytotoxic activity against a wide range of mammalian cell types such as erythrocytes, granulocytes, monocytes, and endothelial cells (Menestrina et al., 2001). The cytotoxic properties of α-HL are mediated by the formation of a wide heptameric channel of 234 kDa. The α-HL monomers insert into the membrane of susceptible cell such as blood monocytes, human platelets, or endothelial cells, and then oligomerize to form a heptameric transmembrane pore, inducing the release of interleukin-1 in vivo (Song et al., 1996; May et al., 1996). The primary mechanism of cell damage and death is a leakage of ions, water, and low molecular weight molecules in and out the cell (Alouf and Freer, 1999; Menestrina et al., 2001).

The high resolution x-ray structure (1.9 Å) shows that one α-HL subunit is composed of 16 β-strands, four turns of α- or $3_{10}$-helix, and substantial non α- or non β-elements of the polypeptide structure for protomer (Song et al., 1996). The mushroom-shaped heptamer of α-HL is ~100 Å in diameter and height (see Fig. 1). The size of the aqueous pore ranges from 15 to 46 Å (Gouaux, 1998; Song et al., 1996). The channel displays a weak anion selectivity, with rapid fluctuations to a higher conduction state at acidic pH (Kasianowicz and Bezrukov, 1995). Slow, reversible, voltage-dependent channel closure can be induced by the presence of di- and trivalent cations (Kasianowicz et al., 1999). Site-directed mutations in the channel interior such as K147N or M113P make the channel moderately cation selective (Gu et al., 2001a,b). The features of this wide aqueous pore make it possible to use α-HL for construction of biosensors, i.e., detecting elements that could become part of a stable device. To modulate the selectivity of the pore, suitable molecules (adaptors) have been used to create a narrow constriction with specific selectivity (Bayley and Martin, 2000; Gu et al., 2001a, 1999).

The availability of a high resolution crystal structure (Song et al., 1996) and wealth of electrophysiological

*Submitted April 2, 2004, and accepted for publication June 14, 2004.*

Address reprint requests to Benoît Roux, Dept. of Biochemistry & Structural Biology, Weill Medical College of Cornell University, 1300 York Ave., New York, NY 10021. Tel.: 212-746-6018; Fax: 212-746-4843; E-mail: benoit.roux@med.cornell.edu.

S.N. is on leave from the Institute of Solution Chemistry, Russian Academy of Sciences, Ivanovo 153045, Russian Federation.



0006-3495/04/10/2299/11 $2.00

doi: 10.1529/biophysj.104.044008

FIGURE 1 Molecular graphics view of the GCMC/BD simulation of the $\alpha$-hemolysin pore bathed in 1.0 M KCl solution. Saggital section of the channel along the Z axis. The orthorhombic simulation box and the 3.0 Å regions corresponding to the buffer areas are drawn as cyan lines. The membrane is delimited by thick white lines. $K^+$ (*magenta*) and $Cl^-$ (*green*) ions are located in the pore and in the buffer regions.

experimental data (Alouf and Freer, 1999) make $\alpha$-HL an ideal system to investigate the microscopic interactions governing ion flow and selectivity in wide aqueous molecular pores. A deeper understanding of the molecular determinants for ion permeation can be achieved by combining the available experimental information on the transport and structural properties of this toxin with detailed theoretical studies (for a recent review, see Roux et al., 2004). The size of the $\alpha$-HL channel (more than 30,000 atoms including hydrogens for protein itself) renders studies of the permeation process using all-atom molecular dynamics (MD) simulations extremely challenging. Shilov and Kurnikova (2003) have recently carried out MD simulations of the cyclic oligosaccharide $\beta$-cyclodextrin dynamics in the confined environment of the $\alpha$-HL channel, freezing the channel atoms to restrict the size of the system. A trajectory of 8 ns was generated to address important questions about the fast dynamical motions of the ligand bound to the channel. Nonetheless the simulation of ion permeation requires much longer trajectories, on the microsecond timescale.

Brownian dynamics (BD) simulation, in which the solvent is represented implicitly, provides an attractive theoretical approach for the modeling of permeation process in wide and medium sized pores over long timescales (Chung et al., 1998; Roux et al., 2004). In this approach, the channel and ions are represented explicitly at the atomic level, but the influence of the surrounding solvent is incorporated implicitly via stochastic random forces and a multi-ion potential of mean force (PMF) approximated on the basis of a continuum dielectric solvent. Recently, a grand canonical Monte Carlo Brownian dynamics (GCMC/BD) algorithm was developed and implemented for simulations of ion channels under various conditions of transmembrane potential and ion concentration (Im et al., 2000; Im and Roux, 2001, 2002a,b). In the case of BD as well as for MD simulation, the properties of the system are extracted from time averages taken over atomistic trajectories. Alternative to simulations is the use of Poisson-Nernst-Plank electrodiffusion theory in three dimension (3d-PNP) based on a mean-field continuum electrostatic approximation (Kurnikova et al., 1999). The theory solves self-consistently for the nonequilibrium ion density (from Fick's law) and the electrostatic potential (from Poisson's equation). Using OmpF porin as a benchmark system, the results from a variety of computational approaches were extensively compared (Im and Roux, 2002b). It was found that equilibrium spatial ion distribution calculated from all-atom MD, GCMC/BD, Poisson-Boltzman (PB), and that nonequilibrium ion fluxes calculated from GCMC/BD and 3d-PNP, were in good agreement (though the analysis showed that PNP theory systematically overestimates the ion fluxes relative to BD). This confirms that GCMC/BD, PB, and 3d-PNP are valuable tools for computational studies of wide aqueous biological channels (Roux et al., 2004).

The purpose of this article is to elucidate the microscopic factors governing ion flow through the $\alpha$-HL channel. One additional motivation of this work is to further compare BD and 3d-PNP in the case of a very large bacterial pore such as $\alpha$-HL to establish their range of applicability. The outline of the article is as follows. In the next section (Methodology), we will describe the details of simulations and provide the theoretical background. This section is followed by detailed discussions of ion flow through the $\alpha$-HL at symmetric and asymmetric ionic (KCl) solutions (Results and Discussion). In the last section of the article (Conclusion), we will summarize the main results of the work.

## METHODOLOGY

### Atomic model and GCMC/BD simulation

The theoretical foundation for the treatment presented here can be found in Roux et al. (2004). The three-dimensional structure for $\alpha$-HL was taken from Protein Data Bank (Berman et al., 2000) (Protein Data Bank entry: 7ahl). The protonation was chosen on the basis of pKa calculations (Bashford and Karplus, 1990; Bashford and Gerwert, 1992). All aspartic acid and glutamic acid residues as well as C-terminal groups were deprotonated; arginine, lysine, and N-terminal groups were protonated. Histidine 35 and 259 are protonated on NE2, histidine 144 is protonated on ND1, and histidine 48 is protonated at both NE2 and ND2. The atomic charges were taken from the CHARMM PARAM22 force field (MacKerell et al., 1998). The resulting net charge for $\alpha$-HL was +14 e. The protein was treated as a rigid structure with a dielectric constant of 2 surrounded by a high dielectric solvent ($\epsilon_w$ = 80) and embedded in a 28.2 Å thick membrane ($\epsilon_m$ = 2). The choice of dielectric constant for the aqueous region was motivated by the large size of the pore, which can be safely assumed to be well-represented by a bulk

continuum value (Partenskii and Jordan, 1992a). The value for $\epsilon_p = 2$ is a canonical value in many theoretical studies, though typical values often ranged from 2 to 5 depending on the situation (Simonson and Brooks, 1996; Pitera et al., 2001; Schutz and Warshel, 2001). Recently, it was shown that an increase in $\epsilon_p$ value can cause a small effect on ion profile (Bastug and Kuyucak, 2003) in large and medium sized pores. The value of $\epsilon_p$ is more critical for studies of permeation through narrow pores, where the application of continuum models is questionable anyway (Corry et al., 2003; Nadler et al., 2003).

The channel was positioned along the $Z$ axis with the center of the membrane at $Z = 0$. An atomic system was constructed to perform GCMC/BD simulations using an orthorhombic simulation region (60.5 × 60.5 × 128.5 Å$^3$). This system is depicted in Fig. 1. The salt concentrations of interest were maintained by two 3 Å buffers positioned from −26.75 to −23.75 Å and from 99.75 to 102.75 Å along the $Z$ axis. The stochastic trajectory of the ions with nonuniform diffusion constant profile was generated using the algorithm of Ermak and McCammom (1978),

$$\dot{\mathbf{r}}_i(t) = -\frac{D_i(\mathbf{r}_i)}{k_B T}\nabla_i \mathcal{W}(\mathbf{r}_1, \mathbf{r}_2, \ldots) + \nabla_i D_i(\mathbf{r}_i) + \boldsymbol{\zeta}_i(t). \quad (1)$$

where $\dot{\mathbf{r}}_i$ is the velocity and $\mathbf{r}_i$ is the position of $i$th ion, $D_i(\mathbf{r}_i)$ is the diffusion coefficient at a given ion position, $\mathcal{W}(\mathbf{r}_1, \mathbf{r}_2, \ldots)$ is a multi-ion PMF, and $\boldsymbol{\zeta}_i(t)$ is a Gaussian random noise with $\langle \boldsymbol{\zeta}_i(t)\cdot\boldsymbol{\zeta}_j(0)\rangle = 6D_i(\mathbf{r}_i)\delta_{ij}(t)$. Based on continuum electrostatics, the multi-ion PMF ($\mathcal{W}$) becomes (Im et al., 2000; Im and Roux, 2001)

$$\begin{aligned}\mathcal{W}(\mathbf{r}_1, \mathbf{r}_2, \ldots) = &\sum_{ij} u_{ij}(|\mathbf{r}_i - \mathbf{r}_j|) + \sum_i U_{\text{core}}(\mathbf{r}_i) \\ &+ \Delta\mathcal{W}_{sf}(\mathbf{r}_1, \mathbf{r}_2, \ldots) \\ &+ \Delta\mathcal{W}_{rf}(\mathbf{r}_1, \mathbf{r}_2, \ldots), \end{aligned} \quad (2)$$

where the Cartesian coordinates of the $i$th ion are represented by $r_i$, $u_{ij}$ is the direct ion-ion interaction, $U_{\text{core}}$ is a repulsive potential preventing core-core overlap of the ions with the channel and membrane, $\Delta\mathcal{W}_{sf}$ is the shielded static field coming from the permanent protein charge distribution and the transmembrane potential, and $\Delta\mathcal{W}_{rf}$ is the reaction field arising from the electrostatic polarization of the various dielectric boundaries and the implicit salt in the outer region (Im and Roux, 2002a).

The static-field electrostatic potential $\Delta\mathcal{W}_{sf}$ was computed first on a coarse grid ($205^3$ points with a grid spacing of 1.5 Å) centered on the origin of the membrane region followed by a second calculation on a finer grid (205 × 205 × 261 points with a grid spacing of 0.5 Å). The transmembrane potential contribution was calculated with a modified version of PB equation (Roux, 1997). This grid completely covers the atomic structure of the α-HL channel. $\Delta\mathcal{W}_{rf}$ is calculated using a generalized basis-set expansion with Legendre polynomials of 5, 5, and 9 order in $X$, $Y$, and $Z$ directions, respectively. A singular value decomposition with optimal cutoff eigenvalue of 0.003 was used to regularize the basis sets (Im and Roux, 2001). The same grid as for $\Delta\mathcal{W}_{sf}$ was used for the calculation of the reaction field matrix. The GCMC/BD simulation trajectories were generated with a time step of 15 fs using the algorithm described by Im and Roux (2002a). One step of GCMC was performed for each step of BD. The step of GCMC essentially adds no computational cost to the BD itself. To examine the current-voltage relation (I-V curve) 1.0 M (symmetric), KCl solutions were maintained in both buffer regions with a transmembrane potential of $V_{mp}$ = −150, −100, −40, 40, 100, and 150 mV. For conductance-concentration relation, the single-channel conductance was calculated at $V_{mp} = \pm 150$ mV in 0.1, 0.2, 0.3, 0.5, 1.0, and 2.0 M KCl solutions. The total length of the simulation was 6 μs (0.1 M), 3.6 μs (0.15 M and 0.2 M), 1.8 μs (0.3 M), 0.9 μs (0.5 M), 0.45 μs (1.0 M), and 0.225 μs (2.0 M) for various symmetric solutions of KCl, and 0.9 μs for asymmetric solutions of KCl. To obtain statistical convergence on the ion currents at given condition, 10 independent GCMC/BD simulations were generated with both different initial configurations and different seed number for the random number generator. All computations have been done using the GCMC/BD program package, which is freely available at http://thallium.med.cornell.edu/RouxLab/gcmc.html.

The same protein model and ion diffusion coefficient profile as used in the GCMC/BD simulation were used for all 3d-PNP computations. One cycle of a 3d-PNP iteration consists of solving the Poisson equation for the electrostatic potential, and the steady-state Nernst-Plank equation for concentration of each ion type. (For details and algorithm of 3d-PNP computations, see Kurnikova et al., 1999, and Im and Roux, 2002a.) Both equations were solved completely for each iterative step of 3d-PNP with tolerance of $4 \times 10^{-6}$ for the potential and $1 \times 10^{-10}$ for the concentrations. Different mixing factors were applied to the potential and concentrations due to high sensitivity of the NP equation for a small changes in potential. All computations were done using the PB/PNP program package, which is freely available at http://thallium.med.cornell.edu/RouxLab/pbpnp.html.

## Position-dependent diffusion coefficient

One of the inputs for GCMC/BD simulation is the position-dependent (nonuniform) ion diffusion coefficient. It is generally accepted that the mobility of ions in a confined environment and in bulk solution are different (Allen et al., 1999). The diffusion coefficient of ions insid a water-filled pore is expected to be influenced by complex effects, including hydrodynamic and electrostatics. MD simulations of hydrophobic channels done by Allen et al. (1999) and Im and Roux (2002a) showed a dependence of ion motion on the channel size. Hydrodynamic effects on ion diffusion are expected to provide a reasonably accurate approach for studies of the ion flow in large pore complexes (for a review, see Peters, 1986).

According to the Stokes-Einstein theory, the diffusion coefficient of a spherical particle (ion) with a radius of $R_{\text{ion}}$ in a bulk liquid with viscosity $\eta$ is

$$D_{\text{ion}} = \frac{k_B T}{6\pi\eta R_{\text{ion}}}. \quad (3)$$

where $k_B$ is the Boltzmann constant, $T$ is the temperature, and $\eta$ is the viscosity of media.

An approximate approach to introduce the dependence of the channel size on the diffusion coefficient of a spherical particle using continuum hydrodynamics were formulated by Paine and Scherr (1975), and was used for calculations of ion transport through cylindrical pores of different size (Paine et al., 1975; Peters, 1986; Keminer and Peters, 1999). The position-dependent diffusion coefficient of the particle inside the cylindrical pore can be written as

$$D_{\text{ion}}(r) = \frac{k_B T}{6\pi\eta R_{\text{ion}} k_1}, \quad (4)$$

where the component friction coefficient $k_1$ is a function of $R_{\text{ion}}$, the radius of the cylindrical pore $R_{\text{pore}}$, and the radial distance of the particle from the central axis of the pore $d$. Combining Eqs. 3 and 4, we can write the position-dependent diffusion constant with respect to the bulk value as

$$D_{\text{ion}}(r) = \frac{D_{\text{ion}}}{k_1}. \quad (5)$$

The magnitude of $k_1$ was tabulated as a function of $\beta = R_{\text{ion}}/R_{\text{pore}}$ (Paine and Scherr, 1975). To simply incorporate $k_1(\beta)$ into the BD algorithm we use an analytical expression such as

$$D_{\text{ion}}(r) = \frac{D_{\text{ion}}}{(A + B\exp(\beta/C) + D\exp(\beta/E)}. \quad (6)$$

The best fit to the tabulated values was obtained with $A = 0.64309$, $B = 0.00044$, $C = 0.06894$, $D = 0.35647$, and $E = 0.19409$.

The channel radius, $R_{pore}$, used in Eq. 5 was extracted from the representation of the channel as a series of ideal cylinders with a different radius. To obtain the cross-sectional area of such cylinders, we used an algorithm similar to that proposed by Smart et al. (1993). The position of an uncharged sphere with minimal van der Waals radius of 0.5 Å was initially optimized at the point of interest inside the channel with a strong harmonic restraint to hold the sphere along the main channel axis. Energy minimization was performed while the van der Waals radius of the sphere was gradually increased by 0.01 Å until the interaction energy between the channel and the sphere reached the value of $k_BT$. Assuming the spherical symmetry of the pore, the radius of the sphere is then taken as the pore radius. To examine the validity of the diffusion coefficient calculated by the simple hydrodynamic model, the position-dependent diffusion constant of ion through OmpF biological channel calculated by Eq. 5 was first compared with that extracted from the MD simulation (Im and Roux, 2002b). As shown in Fig. 2, the simple hydrodynamic model indicates that there is a slight reduction of the diffusion constant in the pore relative to the bulk value, in reasonable agreement with available results from all-atom MD simulation (Im and Roux, 2002b). The agreement is far from perfect, but it should be noted that the value of the ion diffusion coefficient computed from MD is also burdened by some uncertainty (Im and Roux, 2002b). Using the estimated diffusion constant profile for $\alpha$-HL does improve the results by 10–15%. Since ion conduction properties are generally dominated by the multi-ion PMF rather than the diffusion coefficient profile (Roux et al., 2004), the simple hydrodynamic approximation allows a rough and inexpensive estimate for BD simulations in the case of wide pores of complex geometries. Fig. 3 *a* shows the cross-sectional area of $\alpha$-HL calculated by the aforementioned method and a grid search method. The representation of the channel as a set of cylinders slightly underestimates the cross-sectional area, though the agreement between the two different approaches remains acceptable. Finally, Fig. 3 *b* shows the fractional (nonuniform) diffusion constant profile for the spherical particle with a mean radius of $K^+$ and $Cl^-$ inside the $\alpha$-HL pore calculated from the hydrodynamic approximation, and smoothed one for the GCMC/BD and PNP computations. For the sake of simplicity, the variation of the diffusion constant in the $x,y$ plane as well as its small dependence on a salt concentration are neglected in the simulation presented here.

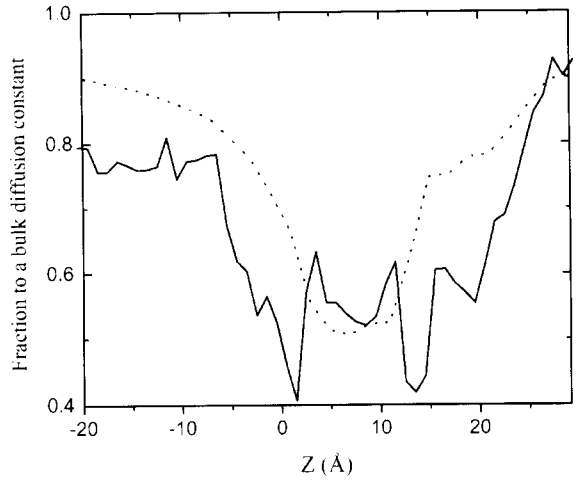


FIGURE 2 Relative diffusion coefficient of $Cl^-$ ion along OmpF channel axis from MD simulations (*solid line*) and hydrodynamic approximation (*dotted line*). The results for the $K^+$ diffusion coefficient profile are similar and not shown here.

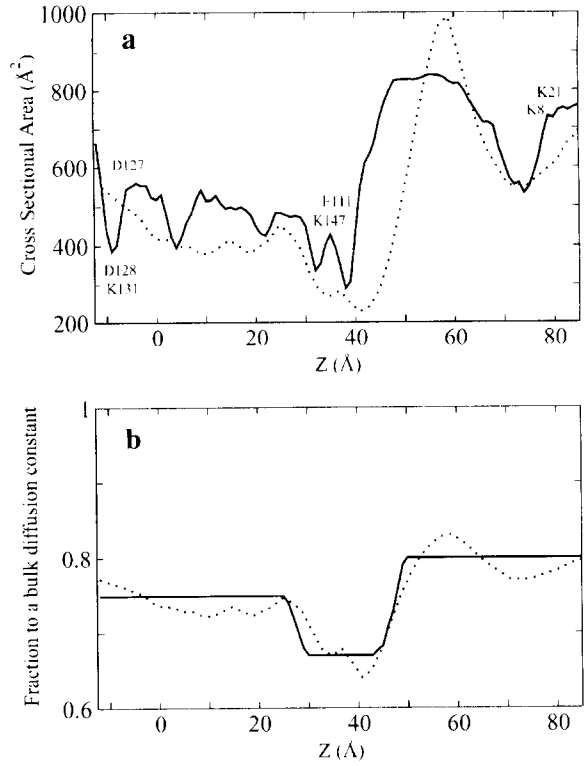


FIGURE 3 (*a*) Cross-sectional area of $\alpha$-HL computed by a grid search (*dotted line*) and evaluated using a variable probe sphere moving along the channel axis (*solid line*). (*b*) Diffusion coefficient relative to a bulk value estimated by a hydrodynamic approximation (*dots*) and used in the BD and PNP computations (*solid line*). The center of the membrane is located at $Z = 0.0$ Å.

## RESULTS AND DISCUSSION

In the following section, we present the results of the equilibrium and nonequilibrium ion flows in the $\alpha$-HL channel, and compare those with available experimental data. The purpose of this comparison is to ascertain the reliability of the GCMC/BD and PNP results and to draw a meaningful picture of ion permeation and selectivity through large and medium sized pores with a high level of details.

### Equilibrium ion distribution

Fig. 4 shows the equilibrium distribution of $K^+$ and $Cl^-$ along the pore axis obtained from the GCMC/BD simulation and the PB calculation. The agreement between the two approaches is remarkable, indicating that the mean-field approximation used in PB is sufficiently good for the description of the equilibrium ion distribution in the wide pore. The distributions for both ions inside the channel are very similar except for minor differences near the wide region in the extracellular part (from 40 to 60 Å) and the narrow end of the stem near the intracellular region (from −14 to 0 Å) (see also Figs. 1 and 2). The average number of ions inside the pore is 22.9 and 23.2 from GCMC/BD, and

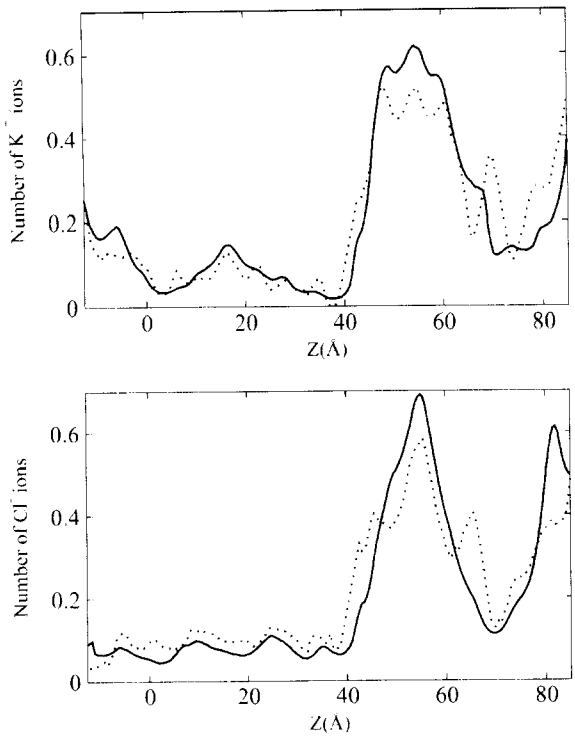


FIGURE 4 Average number of ions inside the channel pore along the $Z$ axis from PB (*dotted line*) and BD (*solid line*). Three major regions can be distinguished: the wide and irregularly shaped extracellular vestibule (87–40 Å), the narrow constriction zone located at the stem neck (40–36 Å) and the long intracellular stem part of the channel (36 to −13.5 Å) formed by $\beta$-strands. The center of the membrane is located at $Z = 0.0$ Å.

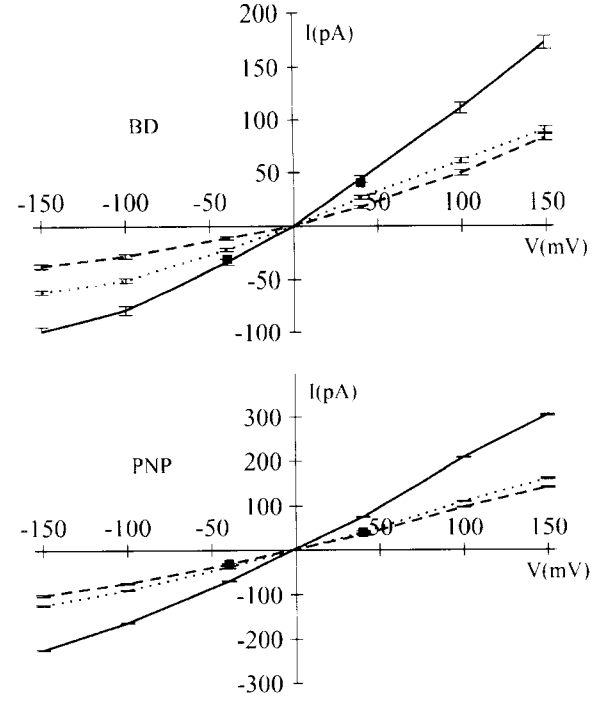


FIGURE 5 Current-voltage relation in a 1.0 M KCl symmetric solution from GCMC/BD simulation and 3d-PNP computations. The total current (*solid line*) is the sum of $K^+$ (*dashed line*) and $Cl^-$ (*dotted line*) currents. Experimental data (■) corresponding to the total current at $V = 40$mV and $V = -40$mV were taken from Menestrina (1986) and Miles et al. (2002), respectively.

21.4 and 23.0 from PB for $K^+$ and $Cl^-$, respectively. In accord with experimental observations (Menestrina, 1986), the channel is very weakly selective for anions. The weak anion selectivity arises from the permanent charge distribution inside the pore. In the wide extracellular part of the channel, both GCMC/BD and PB show a higher propensity for $Cl^-$, whereas the narrow intracellular end displays a preference for $K^+$. A peak in $Cl^-$ density (slightly separated from that for $K^+$) is observed near the wide extracellular part around 78–85 Å along the $Z$ axis. The position of this peak is correlated with two positively charged lysine residues (K8 and K21) in the channel interior (see Fig. 1). There is a significant decrease in the ion accessible area on the extracellular region, which results in some loss of the ionic densities there. A high $K^+$ density peak is observed near the outer rim of the $\beta$-barrel above the two acidic residues (D127 and D128) located between 0 and −12 Å along the $Z$ axis. Because of the heptameric symmetry, there is no significant lateral separation of the anionic and cationic permeation pathways, such as observed for OmpF porin (Im and Roux, 2002a,b).

## Nonequilibrium ion flow: channel conductance

The current-voltage (I-V) relation in the symmetric 1.0 M KCl solution from GCMC/BD and 3d-PNP is shown in Fig. 5. The error bars in the figure represent the root mean-square deviation of 10 independent GCMC/BD runs and numerical errors of the 3d-PNP computations. The I-V relation appears to be asymmetric, i.e., both $I_K$ and $I_{Cl}$ are always larger at positive potential than at the corresponding negative potential. The experimentally measured conductance of the protein inserted into a planar lipid bilayer with a 1.0 M KCl solution is 0.775 nS (Miles et al., 2002), 0.651 nS (Gu and Bayley, 2000) at −40 mV, and 1.01 nS (Menestrina, 1986), and 0.721 nS at +40 mV (Gu and Bayley, 2000). The corresponding values from GCMC/BD simulation at −40 and +40 mV are 0.839 nS and 1.11 nS, with inclusion of hydrodynamic correction in Eq. 5, and 0.946 nS and 1.22 nS, using the bulk diffusion coefficient. In all experimental measurements and theoretical computations cited above, the same transmembrane potential convention was used. The *cis* compartment was connected to the virtual ground and the sign was defined accordingly. Introducing the diffusion coefficient correction does not change the form of the I-V function but only decreases the magnitudes of the flux. The predicted conductance from GCMC/BD is slightly higher than the experimental data. Nonetheless the agreement is remarkable given the fact that no parameters were specifically adjusted to reproduce the experimental values. The corresponding values calculated by 3d-PNP theory are 1.71 ± 0.026 nS and 2.34 ± 0.047 nS. Although the GCMC/BD and PB are in reasonable agreement for the equilibrium ion

density distributions (see Fig. 4), Fig. 5 shows that the ionic currents calculated from 3d-PNP are significantly larger than those from GCMC/BD and experiment by 30–60%. It was shown previously that BD and PNP could yield qualitatively similar results in the case of large pores with simple cylindrical geometries (Moy et al., 2000; Corry et al., 2000), overestimated fluxes by PNP were observed in a study of the OmpF porin (Im and Roux, 2002a). Given that the microscopic model and all input parameters are identical in our GCMC/BD and 3d-PNP calculations, this demonstrates that the origin of such overestimation must arise from the lack of some dynamical ion-ion correlations in the mean-field 3d-PNP theory.

The calculated channel conductance ($G = I/V$) and ion current ratio ($I_K/I_{Cl}$) in various KCl solutions with the transmembrane potentials of $V_{mp} = \pm 150$ mV are summarized in Table 1. Fig. 6 *a* illustrates the conductance-concentration relation at $V_{mp} = 150$ mV. The relation drastically changes from a nonlinear behavior to a linear one at high concentration. This is normally interpreted as indicative of the importance of electrostatics at low concentrations. The single-channel conductance normalized by salt concentration ($G/c$) is shown in Fig. 6 *b*. It appears that ($G/c$) function is well correlated with the average number of ions inside the channel normalized by salt concentration ($N_{pore}/c$), as shown in Fig. 6 *c*.

Table 1 also shows the variation of the asymmetry in the channel conductance upon the polarity of the applied potential, $G_+/G_-$, as a function of the concentration. It appears that the asymmetry decreases with an increase of salt concentration. Similar observations were made in the GCMC/BD simulations of the OmpF porin (Im and Roux, 2002a). This result correlates well with experiment. The experimental conductance asymmetry ($G_+/G_-$) of $\alpha$-HL is 2–3 in 0.1 M KCl (Menestrina, 1986; Walker et al., 1992) and 1.1–1.4 in 1.0 M KCl (Menestrina, 1986; Miles et al., 2002; Gu and Bayley, 2000), respectively. The corresponding values in 0.1 M from GCMC/BD (6.33) and 3d-PNP (7.45) appear to be strongly overestimated. The origin of this effect is unclear. Increasing the salt concentration from 0.1 to 1.0M KCl yields improvement in the computed conductance asymmetries from GCMC/BD (1.74) and PNP (1.59), compared with the experimental value (1.3). An additional cause for the slightly overestimated asymmetry is the transmembrane potential. For instance, the asymmetry computed in 1M of KCL at $V_{mp} = \pm 40$ mV is 1.32, which is the same as the experimental estimate, while increasing the applied potential from 40 mV to 150 mV increases computed asymmetry by 30–50%. Larger values of the transmembrane potential were used here to get better statistics on the ion crossings events from the BD simulations. This is more critical for small concentrations (<0.5 M of KCL). Interestingly, the large bacterial channels such as meningococcal PorA/C1 (Song et al., 1999), MscS (Sukharev, 2002) display also an asymmetric current. Experimental studies of the antibody binding to the meningococcal PorA/C1

**TABLE 1 Conductance (nS) and current ratios from GCMC/BD simulations and PNP calculations of $\alpha$-HL in various KCl symmetric solutions**

| | $V_{mp} = +150$ mV | | | $V_{mp} = -150$ mV | | | |
|---|---|---|---|---|---|---|---|
| Concentration (M) | $G_+$ | | $I_K/I_{Cl}$ | $G$ | | $I_K/I_{Cl}$ | $G_-/G$ |
| GCMC/BD | | | | | | | |
| 2.00 | 2.02 ± 0.060 | | 0.98 | 1.45 ± 0.042 | | 0.69 | 1.39 |
| 1.00 | 1.15 ± 0.041 | (1.00*) (0.721‡) | 0.91 | 0.66 ± 0.029 | (0.77†) (0.651‡) | 0.59 | 1.74 |
| 0.50 | 0.66 ± 0.008 | (0.45*) | 0.94 | 0.27 ± 0.011 | | 0.64 | 2.44 |
| 0.30 | 0.45 ± 0.015 | (0.37*) | 0.98 | 0.13 ± 0.008 | | 0.56 | 3.46 |
| 0.20 | 0.35 ± 0.007 | | 0.94 | 0.075 ± 0.004 | | 0.52 | 4.66 |
| 0.10 | 0.19 ± 0.002 | (0.14*) (0.18§) | 1.09 | 0.031 ± 0.002 | (0.06*) (0.1¶) | 0.47 | 6.12 |
| PNP | | | | | | | |
| 2.00 | 4.08 ± 0.029 | | 0.90 | 3.22 ± 0.037 | | 0.89 | 1.26 |
| 1.00 | 2.38 ± 0.048 | | 0.89 | 1.49 ± 0.012 | | 0.81 | 1.59 |
| 0.50 | 1.19 ± 0.026 | | 0.91 | 0.58 ± 0.010 | | 0.77 | 2.05 |
| 0.30 | 0.79 ± 0.009 | | 0.82 | 0.31 ± 0.007 | | 0.71 | 2.54 |
| 0.20 | 0.55 ± 0.012 | | 1.01 | 0.12 ± 0.011 | | 0.73 | 4.58 |
| 0.10 | 0.31 ± 0.035 | | 1.11 | 0.04 ± 0.004 | | 0.69 | 7.75 |

All numbers representing the experimental conductances are shown in the following potential convention: the *cis* compartment of the experimental chamber was connected to the virtual ground.

Experimental channel conductance is in parentheses:

*Measurements done at applied voltage of 40 mV and different salt solution compositions (Menestrina, 1986).

†Applied voltage of −40mV and 1.0 M of KCl solution (Miles et al., 2002).

‡Applied voltage $V_{mp} = +40$ mV and 1.0M of KCl solution (Gu and Bayley, 2000).

§Applied voltage of 15 mV and 0.1 M of KCl solutions (Walker et al., 1992).

¶Applied voltage of −40 mV and 0.1 M of KCl solutions (Krasilnikov et al., 2000).

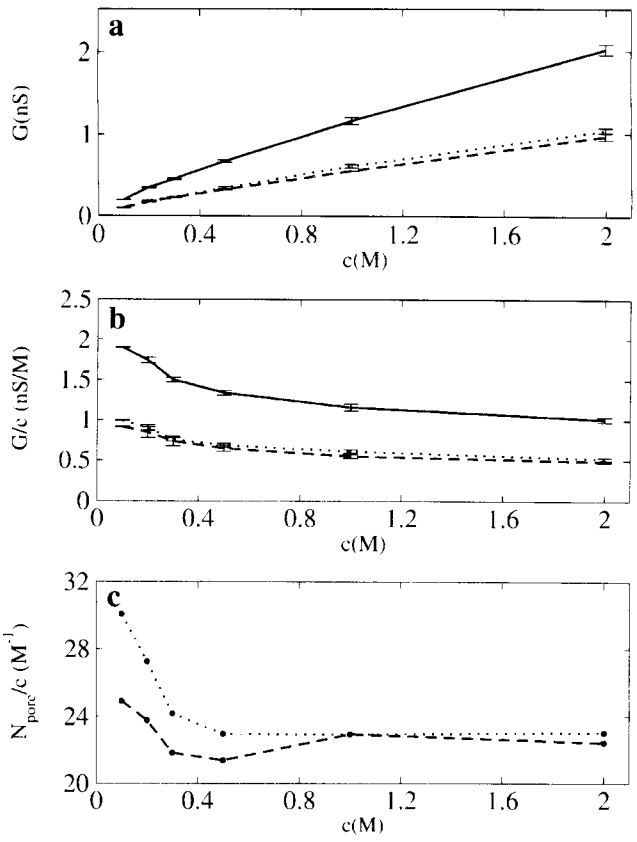


FIGURE 6 (*a*) Conductance-concentration (*G*-*c*) relation (*solid line*) from GCMC/BD at $V_{mp}$ = 150 mV with contribution from $K^+$ (*dashed line*) and $Cl^-$ (*dotted line*) currents. (*b*) Channel conductances normalized by a salt concentration. (*c*) Number of ions $K^+$ (*dashed line*) and $Cl^-$ (*dotted line*) inside the pore normalized by salt concentration from BD simulation without transmembrane potential.

suggested that the rectification of the current could be explained in the terms of the protein shape (Song et al., 1999).

One possible explanation for the asymmetric conductance is the static charge distribution in the channel interior. This is exemplified by the strong dependence of the asymmetry upon salt concentration. An additional factor may be the specific geometry of the pore. To elucidate the origin of the conductance asymmetry of α-HL, we performed GCMC/BD simulations of the channel bathed in 1.0 M KCl solutions with all protein charges turned off at two opposite voltages ($V_{mp} = \pm 150$ mV). The results are 0.98 nS and 0.96 nS at positive and negative voltage, respectively, showing that the shape of the pore has no significant effect on the asymmetric conduction in α-HL.

To elucidate the molecular determinants of the asymmetric channel conductance, we examined the effect of a step-by-step neutralization of different parts of the channel on ion flow. A 0.5M KCl symmetric solution was simulated at ±150 mV with GCMC/BD because the computed and experimentally measured conductances agree reasonably, and asymmetric effects in the ion conductance are well-pronounced in comparison to higher salt concentrations. First, it appears that the neutralization of the wide cap domain of the α-HL does not change significantly the ion permeation properties except for some increase in the ion currents. The cap domain sequence used for neutralization contains up to 80% of all amino acid residues except those forming the transmembrane domain from Lys-110 to Tyr-148 (Song et al., 1996). The channel conductances computed by the GCMC/BD simulations are 0.79 nS at +150 mV and 0.39 nS at −150 mV, which corresponds to a $G_+/G_-$ ratio of 2.02 compared to 2.44 for the fully charged channel. The complete neutralization of the transmembrane stem domain formed by β-barrels clearly shows more pronounced effects on the channel conductance making it almost symmetric at different voltages with a $G_+/G_-$ of 0.98. Assuming that the geometry does not have any significant influence on the asymmetric conductance, we further explored the contributions of different residues located in the stem domain on the channel conductance. Misakian and Kasianowics (2003) suggested that the asymmetric conductance can be attributed to the side chains of E111, which introduces a barrier for the anion passage in the constriction zone of the channel, or to the charges located in or near channel entrances (D127-D128-K131). All results on the ionic currents through the α-HL channel and its partially neutralized forms are collected in Table 2. The complete neutralization of E111 or the E111-K147 ion pair in the constriction zone does not eliminate the asymmetric conduction through the channel but affects its magnitude, i.e., the conduction ratio $G_+/G_-$ is 3.34 and 1.98 for neutralized E111 and E111-K147, respectively. Furthermore, a close examination reveals that the cation current with and without the neutralization of E111 remains almost unchanged at ±150 mV (within the statistical error of the GCMC/BD simulation), but the anion current increases significantly for both voltages in comparison to the wild-type. Our findings suggest that E111 and K147 are essential for the ion selectivity but not for the rectification of the ion current. As shown in Fig. 7 *a*, an energy barrier due to the presence of E111 exists, but it is not rate-determining. Fig. 7 *a* rather suggests that the asymmetry arises from the presence of the potential barrier near the intracellular end of the stem domain, between 0 and −12 Å along the *Z* axis. It also depends on the direction of the salt gradient. The one-dimensional free-energy profiles summarized with the positive (Fig. 7 *b*) and negative (Fig. 7 *c*) transmembrane potential contributions reveal the origins of the asymmetric conduction phenomenon. At negative applied voltage, the barrier located at the end of the transmembrane region is partially compensated by the contribution from the transmembrane potential. Three charged residues (D127, D128, and K131) are located between the 0 and −12 Å zone along the *Z* axis corresponding to the potential barrier discussed above. D127 and K131 form an ionic pair, and D128 provides an additional negative charge. This affects the shape of the I-V

**TABLE 2 Ion currents (pA) and conductance (nS) from GCMC/BD simulations of $\alpha$-hemolysin channel and its partially neutralized forms in 0.5M KCl symmetric solutions**

| Protein | $V_{imp} = +150$mV | | | | $V_{imp} = -150$mV | | | | |
|---|---|---|---|---|---|---|---|---|---|
| | $I_K(+)$ | $I_{Cl}(-)$ | $I_K/I_{Cl}$ | $G_+$ | $I_K(-)$ | $I_{Cl}(+)$ | $I_K/I_{Cl}$ | $G_-$ | $G_+/G$ |
| Wild-type | 47.97 | 51.03 | 0.94 | 0.66 | −15.81 | −24.69 | 0.64 | 0.27 | 2.44 |
| E111 | 54.47 | 136.17 | 0.40 | 1.27 | −10.68 | −46.46 | 0.22 | 0.38 | 3.34 |
| K147 | 83.31 | 18.69 | 4.45 | 0.68 | −93.46 | −33.11 | 2.82 | 0.84 | 0.81 |
| E111-K147 | 89.67 | 40.83 | 2.2 | 0.87 | −27.38 | −39.72 | 0.68 | 0.44 | 1.98 |
| D127 | 29.90 | 66.24 | 0.45 | 0.64 | −37.41 | −103.31 | 0.36 | 0.93 | 0.48 |
| D128 | 42.99 | 77.42 | 0.55 | 0.80 | −33.61 | −85.20 | 0.39 | 0.79 | 0.99 |
| K131 | 91.25 | 89.36 | 1.02 | 1.2 | −28.94 | −40.72 | 0.71 | 0.46 | 2.61 |
| D127-D128-K131 | 34.96 | 91.61 | 0.38 | 0.84 | −33.82 | −94.34 | 0.35 | 0.85 | 0.99 |

$I_\alpha(+)$ and $I_\alpha(-)$ are outward and inward currents of the ion type $\alpha$, respectively.

curve and introduces the asymmetries in the ionic conduction through $\alpha$-HL. The acceleration of the cation is the result of the electric field from the D128 in addition to the ionic pair formed by D127 and K131, i.e., D128 makes the intracellular entrance of the channel attractive for cations and introduces the asymmetry in the conductance. To test these ideas, additional simulations were performed in which the side chains of D127, D128, and K131 were neutralized. The calculated $G_+/G_-$ for neutralized side chains of D127, D128, and K131 are 0.48, 0.99, and 2.61 respectively. These results demonstrate conclusively that the presence of D128 near the intracellular end is the molecular determinant of the asymmetric channel conductance in $\alpha$-HL.

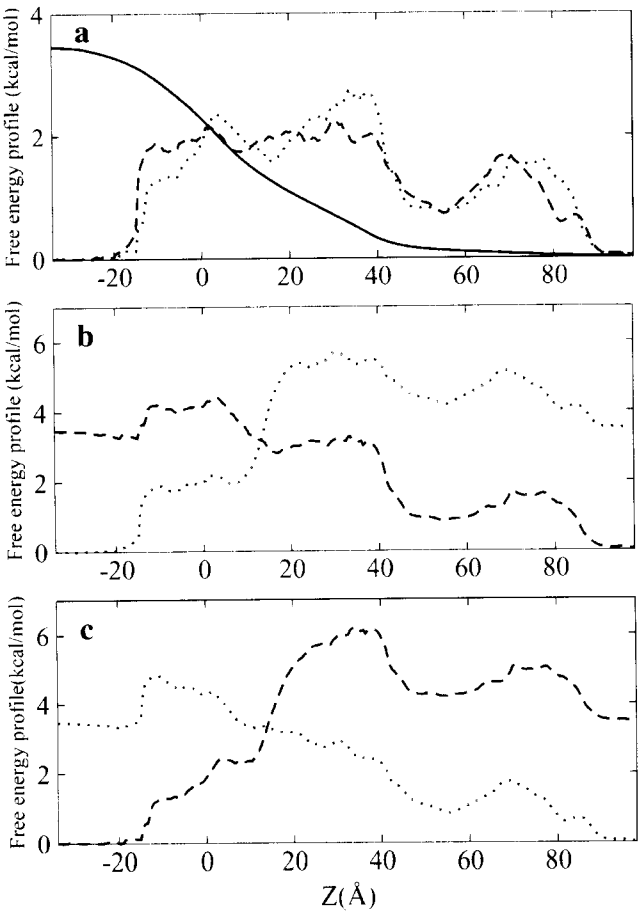


FIGURE 7 (*a*) Effective one-dimensional free-energy profile of $K^+$ (*dashed line*), $Cl^-$ (*dotted line*), and the transmembrane potential (*solid line*) in a 1.0 M KCl symmetric solution. The center of the membrane is located at $Z = 0.0$ Å. The same profile combined with contribution from transmembrane potential of (*b*) +150mV and (*c*) −150mV.

## Nonequilibrium ion flow: channel selectivity

A generally accepted framework to characterize the selectivity of ion channels is the Goldman-Hodgkin-Katz voltage equation for the reversal potential $V_{rev}$ (Hodgkin and Katz, 1949),

$$V_{rev} = \frac{k_B T}{e} \ln\left[\frac{P_K[C]_o + P_{Cl}[C]_i}{P_K[C]_i + P_{Cl}[C]_o}\right], \quad (7)$$

where $[C]_i$ and $[C]_o$ are the intracellular and extracellular KCl concentrations.

Im and Roux (2002a) suggested that the current ratio $I_K/I_{Cl}$ can be used as an indicator for the selectivity at a given concentration. As shown in Table 1, the distribution of $I_K/I_{Cl}$ suggests that ion concentrations have no visible influence on channel selectivity, though selectivity depends on the direction of the salt gradient. This agrees qualitatively with the experimental observations reported by Gu et al. (2001a,b), where the permeability ratio ($P_K/P_{Cl}$) is 0.34–0.55 for $[C]_i = 0.2$:$[C]_o = 1.0$ M KCl and 0.79 for 1.0:0.2M KCl. Those values correspond to a normal range of pH 5.5 to 7.5 (Gu et al., 2001a,b). According to experiments, the pore displays a very similar preference in the case of NaCl, with measured permeability ratio of 0.78 (Gu et al., 2003). For a more rigorous analysis, the permeability ratio is extracted from the reversible potentials in Figs. 8 and 9. As shown in Table 3, the results are 0.515 (GCMC/BD) and 0.553 (3d-PNP) for 0.2:1.0 M KCl, and 0.971 (GCMC/BD) and 1.322 (3d-PNP) for 1.0:0.2M KCl, which are in excellent accord with the experimental values.

Both computations and experimental observations show that the direction of the salt gradient has a significant effect

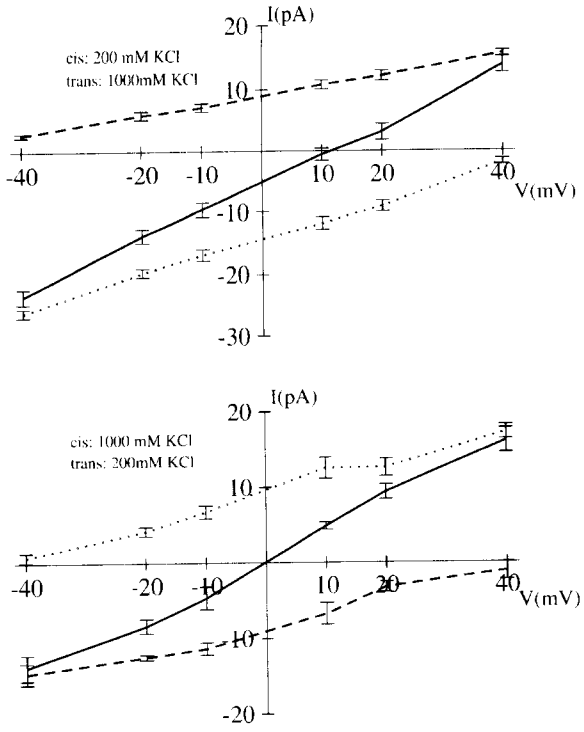


FIGURE 8 Current-voltage relation in KCl asymmetric solution from GCMC/BD simulations. The total current (*solid line*) is the sum of $K^+$ (*dashed line*) and $Cl^-$ (*dotted line*) currents.

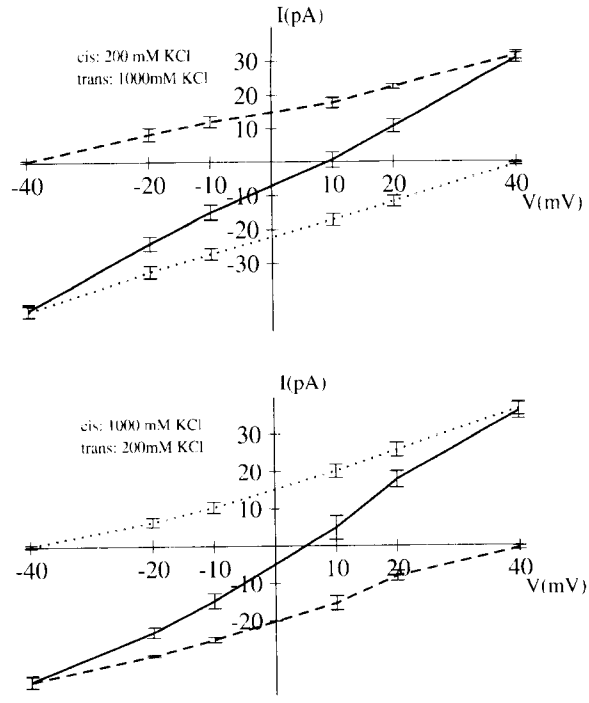


FIGURE 9 Current-voltage relation in KCl asymmetric solution from PNP computations. The total current (*solid line*) is the sum of $K^+$ (*dashed line*) and $Cl^-$ (*dotted line*) currents.

on the permeability ratio. This might be attributed to a nonsymmetric free energy profile of ions inside the channel. As discussed above, there is a moderate separation in the magnitude of the energetic barriers for anions and cations near the narrow stem region, which favors cation passage due to D128. An additional barrier at the wide extracellular part opposes extracellular-to-intracellular cation passage when $[C]_l = 0.2$M and $[C]_o = 1.0$ M KCl. The extracellular anion-attractive side has an average radius twice larger than that of the narrow stem part (Fig. 3). This results in an increase of the number of anions, which is not completely compensated by the changes of the salt gradient from 1.0:0.2 M to 0.2:1.0 M KCl. The delicate balance between these two effects results in the decrease or even reverse of channel selectivity to a nonselective (GCMC/BD) or weak-cation selective (3d-PNP) form with the change of the salt gradient directions from 1.0:0.2 M to 0.2:1.0 M KCl. It should be noted that the standard error in the reversal potential extracted from GCMC/BD simulation or 3d-PNP computations at the small voltages is generally high, and it is difficult to define small reversal potentials more accurate than ±2–3 mV. A similar uncertainty exists for the experiments.

The free energy profiles in Fig. 7 clearly show that the effective free-energy barriers are smaller by 0.5–1 kcal/mol for anions compared to cations except near the narrow intracellular end of the channel, which makes the channel anion-selective. The highest energetic barrier is located near 35–40 Å, i.e., in the narrowest part of the channel (the constriction zone) formed by the pair of two charged residues E111 and K147.

The results on the current ratio $I_K/I_{Cl}$ as an indicator for selectivity accumulated in Table 2 suggest that the ion pair of E111 and K147 is causing the weak anion selectivity. To test this, we performed a series of GCMC/BD simulations in the asymmetric 0.2:1.0 M KCl solution with the charges of those side chains turned off. The neutralization of E111 resulted in high anion selectivity, with a reversal potential extracted from an I-V relation of 25.6 mV and a permeability ratio of 0.185. Similar computations done with a neutralized K147 result in a moderate cation selectivity, with a reversal potential of −17.8 mV and permeability ratio of 2.975. The neutralization of E111 and K147 result in a nonselective channel, with a reversal potential of 0.5 mV and a permeability ratio of 0.971. Wild-type channel at similar conditions displays a reversal potential of 9.2 mV with a permeability ratio of 0.515. Experimentally, an increase of anion selectivity is observed in low pH values (Menestrina, 1986). This may be attributed to the possible protonation

**TABLE 3 The reversal potential ($V_{rev}$ in mV) and permeability ratio ($P_K/P_{Cl}$)* of the α-hemolysin channel**

| Composition | GCMC/BD | PNP | Experiment |
|---|---|---|---|
| 0.2M:1.0M | 11.20 (0.51) | 10.05 (0.55) | 9.2 (0.55) |
| 1.0M:0.2M | −0.50 (0.97) | 4.60 (1.32) | −3.7 (0.79) |

*Corresponding permeability ratios are in parentheses.

of E111, which affects the cumulative positive charge on E111-K147 salt bridge and makes the pore more attractive to anions.

The crystal structure shows that the positively charged side chain of K147 points toward the lumen of the pore, whereas the negatively charged side chain of E111 located along the channel axis form a salt bridge with K147. The average distance between the NZ amide group of K147 and the central axis of the channel is 7 Å. The corresponding distance for the carboxylate group of E111 is 9 Å. The specific position of K147 in the constriction zone makes the channel surface more attractive for anions than for cations, but this effect is moderated by the presence of E111 located next to K147. This finding is in excellent agreement with experimental studies of the single amino-acid replacement in the $\alpha$-HL channel, where the single mutation K147N made the channel moderately cation selective, whereas the double mutation E111N/K147N did not show any ion selectivity (Gu et al., 2001a,b). It was shown that these residues are not conserved in the hemolysin-like proteins and their simultaneous replacement by cysteines does not affect the function of the protein significantly (Gouaux, 1998). It can be concluded that the small charge separation presented by the salt bridge in the constriction zone of the channel is the reason of the weak anion selectivity.

## CONCLUSION

We have performed extensive computations of ion permeation through the $\alpha$-HL channel to elucidate the origins of the asymmetric conductance and the structural basis of the weak anion selectivity of the channel. It was found that the molecular determinant of the asymmetry in the conduction is the presence of the potential barrier located at the intracellular side of the $\beta$-barrel. This barrier is caused by the unpaired negatively charged residue D128 located near the intracellular entrance to the channel. Together with the direction of the applied transmembrane potential, it provides a significant acceleration for cation flow through the channel and therefore affects the symmetry in ion conduction. In addition, the charged separation in the constriction zone of the channel due to the presence of E111 and K147 was identified as the structural feature at the origin of the anion selectivity.

From a methodological point of view, this study demonstrates the overall validity of computational models to simulate ion flow in medium and large aqueous channels. The results obtained using GCMC/BD and 3d-PNP are consistent with available experimental data. This indicates that both methods are able to capture the important electrostatic interactions among ions, solvent, and protein. However, although 3d-PNP reproduces experimentally measured reversal potentials and permeability ratios fairly well, the channel conductance is typically overestimated by 30–50%. Because 3d-PNP (or PB) reproduces the results of GCMC/BD under equilibrium conditions, in the absence of ion flow, the main reason for inaccuracies in PNP is a lack of dynamical ion-ion correlations. How to fix such deficiency is, however, unclear (Roux et al., 2004).

The channel conductances and selectivities from GCMC/BD simulations are in excellent accord with the experimental data. This is particularly satisfying since all inputs for BD such as ionic exclusion hydration layers, water-mediated short-range ionic interactions $w_{sr}(r)$, were extracted from previous MD simulations of the OmpF channel (Im and Roux, 2001, 2002a) and were used without any specific adjustments to reproduce the experimental data for $\alpha$-HL.

Useful discussions with Toby Allen are gratefully acknowledged.

This work was supported by National Institutes of Health grant GM 62342. This project was also funded by a fellowship from the Epilepsy Foundation through the generous support of the American Epilepsy Society and UCB Pharma (Sergei Noskov).

## REFERENCES

Allen, T. W., S. Kuyucak, and S. H. Chung. 1999. The effect of hydrophobic and hydrophilic channel walls on the structure and diffusion of water and ions. *J. Chem. Phys.* 111:7985–7999.

Alouf, J. E., and J. H. Freer. 1999. Comprehensive Sourcebook of Bacterial Protein Toxins. Academic Press, London.

Bashford, D., and K. Gerwert. 1992. Electrostatic calculation of the pKa values of ionizable groups in bacteriorhodopsin. *J. Mol. Biol.* 224:473–486.

Bashford, D., and M. Karplus. 1990. pKa's of ionizable groups in proteins: atomic detail from a continuum electrostatic model. *Biochemistry.* 29: 10219–10225.

Bastug, T., and S. Kuyucak. 2003. Role of the dielectric constants of membrane proteins and channel water in ion permeation. *Biophys. J.* 84:2871–2882.

Bayley, H., and C. R. Martin. 2000. Resistive-pulse sensing-from microbes to molecules. *Chem. Rev.* 100:2575–2594.

Berman, H. M., Z. Westbrook, G. Feng, T. N. Gilliland, H. Bhat, I. N. Weissig, I. N. Shindyalov, and P. E. Bourne. 2000. The protein data bank. *Nucl. Acid. Res.* 28:235–242.

Bhakdi, S., and J. Tranum-Jensen. 1991. Alpha-toxin of staphylococcus aureus. *Microbiol. Rev.* 55:733–759.

Chung, S. H., M. Hoyles, T. Allen, and S. Kuyucak. 1998. Study of ionic currents across a model membrane using Brownian dynamics. *Prog. Biophys. Mol. Biol.* 46:51–96.

Corry, B., S. Kuyucak, and S. H. Chung. 2003. Dielectric self-energy in Poisson-Boltzmann and Poisson-Nernst-Planck models of ion channels. *Biophys. J.* 84:3594–3606.

Corry, B., S. Kuyucak, and S. H. Chung. 2000. Tests of continuum theories as models of ion channels. II. Poisson-Nernst-Plank theory versus Brownian dynamics. *Biophys. J.* 78:2364–2381.

Ermak, D., and J. A. McCammom. 1978. Brownian dynamics with hydrodynamic interaction. *J. Chem. Phys.* 69:1352–1360.

Gentschev, I., G. Dietrich, and W. Goebel. 2002. The *E. coli* alpha-hemolysin secretion system and its use in vaccine development. *Trends Microbiol.* 10:39–45.

Gouaux, E. 1998. Alpha-hemolysin from staphylococcus aureus: an archetype of beta-barrel, channel-forming toxins. *J. Struct. Biol.* 121: 110–122.

Gu, L. Q., and H. Bayley. 2000. Interaction of the noncovalent molecular adapter, beta-cyclodextrin, with the staphylococcal alpha-hemolysin pore. *Biophys. J.* 79:1967–1975.

Gu, L. Q., O. Braha, S. Conlan, S. Cheley, and H. Bayley. 1999. Stochastic sensing of organic analytes by a pore-forming protein containing a molecular adapter. *Nature.* 398:686–690.

Gu, L. Q., M. Dalla Serra, J. B. Vincent, G. Vigh, S. Cheley, O. Braha, and H. Bayley. 2001a. Reversal of charge selectivity in transmembrane protein pores by using noncovalent molecular adapters. *Proc. Natl. Acad. Sci. USA.* 97:3959–3964.

Gu, L. Q., S. Cheley, and H. Bayley. 2001b. Prolonged residence time of a noncovalent molecular adapter, beta-cyclodextrin, within the lumen of mutant alpha-hemolysin pores. *J. Gen. Physiol.* 118:481–494.

Gu, L. Q., S. Cheley, and H. Bayley. 2003. Electroosmotic enhancement of the binding of a neutral molecule to a transmembrane pore. *Proc. Natl. Acad. Sci. USA.* 100:15498–15503.

Hodgkin, A., and B. Katz. 1949. The effect of sodium ions on the electrical activity of the giant axon of the squid. *J. Physiol.* 108:37–77.

Im, W., and B. Roux. 2001. Brownian dynamics simulations of ion channels: a general treatment of electrostatic reaction fields for molecular pores of arbitrary geometry. *J. Chem. Phys.* 115:4850–4861.

Im, W., and B. Roux. 2002a. Ion permeation and selectivity of OmpF porin: a theoretical study based on molecular dynamics, Brownian dynamics, and continuum electrodiffusion theory. *J. Mol. Biol.* 322:851–869.

Im, W., and B. Roux. 2002b. Ions and counterions in a biological channel: a molecular dynamics simulation of OmpF porin from *Escherichia coli* in an explicit membrane with 1 m kcl aqueous salt solution. *J. Mol. Biol.* 319:1177–1197.

Im, W., S. Seefeld, and B. Roux. 2000. Grand canonical Monte Carlo-Brownian dynamics algorithm for simulating ion channels. *Biophys. J.* 79:788–801.

Kasianowicz, J. J., and S. M. Bezrukov. 1995. Protonation dynamics of the alpha-toxin ion channel from spectral analysis of ph-dependent current fluctuations. *Biophys. J.* 69:94–105.

Kasianowicz, J. J., D. L. Burden, S. Han, L. C. Cheley, and H. Bayley. 1999. Genetically engineered metal ion binding sites on the outside of a channel's transmembrane beta-barrel. *Biophys. J.* 76:837–845.

Keminer, O., and R. Peters. 1999. Permeability of single nuclear pores. *Biophys. J.* 77:217–228.

Krasilnikov, O. V., P. G. Merzlyak, L. N. Yuldasheva, C. G. Rodrigues, S. Bhakdi, and A. Valeva. 2000. Electrophysiological evidence for heptameric stoichiometry of ion channels formed by staphylococcus aureus alpha-toxin in planar lipid bilayers. *Mol. Microbiol.* 37:1372–1378.

Kurnikova, M., R. Coalson, P. Graf, and A. Nitzan. 1999. A lattice relaxation algorithm for three-dimensional Poisson-Nernst-Planck theory with application to ion transport through the gramicidin a channel. *Biophys. J.* 76:642–656.

Laestadius, A., A. Richter-Dahlfors, and A. Aperia. 2002. Dual effects of *Escherichia coli* alpha-hemolysin on rat renal proximal tubule cells. *Kidney Int.* 62:2035–2042.

MacKerell, A. D., D. Bashford, M. Bellott, R. L. Dunbrack, J. D. Evanseck, M. J. Field, S. Fischer, J. Gao, H. Guo, S. Ha, D. Joseph-McCarthy, L. Kuchnir, K. Kuczera, F. T. K. Lau, C. Mattos, S. Michnick, T. Ngo, D. T. Nguyen, B. Prodhom, W. E. Reiher, B. Roux, M. Schlenkrich, J. C. Smith, R. Stote, J. Straub, M. Watanabe, J. Wiorkiewicz-Kuczera, D. Yin, and M. Karplus. 1998. All-atom empirical potential for molecular modeling and dynamics studies of proteins. *J. Phys. Chem. B.* 102: 3586–3616.

May, A. K., R. G. Sawyer, T. Gleason, A. Whitworth, and T. L. Pruett. 1996. In vivo cytokine response to *Escherichia coli* alpha-hemolysin determined with genetically engineered hemolytic and nonhemolytic *E. coli* variants. *Infect. Immun.* 64:2167–2171.

Menestrina, G. 1986. Ionic channels formed by staphylococcus aureus alpha-toxin: voltage-dependent inhibition by divalent and trivalent cations. *J. Membr. Biol.* 90:177–190.

Menestrina, G., M. D. Serra, and G. Prevost. 2001. Mode of action of beta-barrel pore-forming toxins of the staphylococcal alpha-hemolysin family. *Toxicon.* 39:1661–1672.

Miles, G., H. Bayley, and S. Cheley. 2002. Properties of *Bacillus cereus* hemolysin II: a heptameric transmembrane pore. *Protein Sci.* 11:1813–1824.

Misakian, M., and J. J. Kasianowicz. 2003. Electrostatic influence on ion transport through the hl channel. *J. Membr. Biol.* 195:137–146.

Moy, G., B. Corry, S. Kuyucak, and S. H. Chung. 2000. Tests of continuum theories as models of ion channels. I. Poisson-Boltzmann theory versus Brownian dynamics. *Biophys. J.* 78:2349–2363.

Nadler, B., U. Hollerbach, and R. S. Eisenberg. 2003. Dielectric boundary force and its crucial role in gramicidin. *Phys. Rev. E.* 68:021905.

Paine, P. L., L. C. Moore, and S. B. Horowitz. 1975. Nuclear-envelope permeability. *Nature.* 254:109–114.

Paine, P. L., and P. Scherr. 1975. Drag coefficients for the movement of rigid spheres through liquid-filled cylindrical pores. *Biophys. J.* 15:1087–1091.

Partenskii, M. B., and P. C. Jordan. 1992a. Nonlinear dielectric behavior of water in transmembrane ion channels: Ion energy barriers and the channel dielectric constant. *J. Phys. Chem.* 96:3906–3910.

Peters, R. 1986. Fluorescence microphotolysis to measure nucleocytoplasmic transport and intracellular mobility. *Biochim. Biophys. Acta.* 864: 305–359.

Pitera, J. W., M. Falta, and W. F. van Gunsteren. 2001. Dielectric properties of proteins from simulation: the effects of solvent, ligands, pH, and temperature. *Biophys. J.* 80:2546–2555.

Roux, B. 1997. The influence of the membrane potential on the free energy of intrinsic protein. *Biophys. J.* 73:2980–2989.

Roux, B., T. Allen, S. Berneche, and W. Im. 2004. Theoretical and computational models of biological ion channels. *Quart. Rev. Biophys.* 37:15–103.

Schutz, C. N., and A. Warshel. 2001. What are the dielectric "constants" of proteins and how to validate electrostatic models? *Proteins.* 44:400–417.

Shilov, I. Y., and M. G. Kurnikova. 2003. Energetics and dynamics of cyclic oligosaccharide molecule in confined protein pore environment. a molecular dynamics study. *J. Phys. Chem. B.* 107:7189–7201.

Simonson, T., and C. L. Brooks. 1996. Charge screening and the dielectric constant of proteins: insights from molecular dynamics. *J. Am. Chem. Soc.* 118:8452–8458.

Smart, O. S., J. M. Goodfellow, and B. A. Wallace. 1993. The pore dimensions of gramicidin A. *Biophys. J.* 65:2455–2460.

Song, J., A. S. A. Conceição, M. Minetti, M. S. Blake, and M. Colombini. 1999. Meningococcal pora/c1, a channel that combines high conductance and high selectivity. *Biophys. J.* 76:804–813.

Song, L., M. R. Hobaugh, C. Shustak, L. Cheley, H. Bayley, and E. Gouaux. 1996. Structure of staphylococcal alpha-hemolysin, a heptameric transmembrane pore. *Science.* 274:1859–1866.

Sukharev, S. 2002. Purification of the small mechanosensitive channel of *Escherichia coli* (MscS): the subunit structure, conduction, and gating characteristics in liposomes. *Biophys. J.* 83:290–298.

Walker, B. J., M. Krishnasastry, L. Zorn, J. J. Kasianowicz, and H. Bayley. 1992. Functional expression of the alpha-hemolysin of staphylococcus-aureus in intact *Escherichia coli* and in cell lysates—deletion of 5 C-terminal amino-acids selectively impair hemolytic-activity. *J. Biol. Chem.* 267:10902–10909.

# Control of ion selectivity in potassium channels by electrostatic and dynamic properties of carbonyl ligands

**Sergei Yu. Noskov[1]*, Simon Bernèche[2] & Benoît Roux[1]**

[1]*Department of Biochemistry & Structural Biology, Weill Medical College of Cornell University, 1300 York Avenue, New York, New York 10021, USA*
[2]*Division of Structural Biology, Biozentrum, University of Basel Klingelbergstrasse 70, CH-4056 Basel, Switzerland*

* Permanent address: Institute of Solution Chemistry, Russian Academy of Sciences, 1 Akademicheskaya street, 153045, Ivanovo, Russia

**Potassium channels are essential for maintaining a normal ionic balance across cell membranes. Central to this function is the ability of such channels to support transmembrane ion conduction at nearly diffusion-limited rates while discriminating for $K^+$ over $Na^+$ by more than a thousand-fold. This selectivity arises because the transfer of the $K^+$ ion into the channel pore is energetically favoured, a feature commonly attributed to a structurally precise fit between the $K^+$ ion and carbonyl groups lining the rigid and narrow pore[1]. But proteins are relatively flexible structures[2,3] that undergo rapid thermal atomic fluctuations larger than the small difference in ionic radius between $K^+$ and $Na^+$. Here we present molecular dynamics simulations for the potassium channel KcsA, which show that the carbonyl groups coordinating the ion in the narrow pore are indeed very dynamic ('liquid-like') and that their intrinsic electrostatic properties control ion selectivity. This finding highlights the importance of the classical concept of field strength[4]. Selectivity for $K^+$ is seen to emerge as a robust feature of a flexible fluctuating pore lined by carbonyl groups.**

Selective conduction of $K^+$ is conferred by the narrowest region of the pore formed by the backbone carbonyl groups of the residue sequence TTVGYG, which is highly conserved among all known potassium channels (Fig. 1)[5–7]. Although equilibrium and non-equilibrium aspects must both be taken into consideration to address this question completely, the observed selectivity of KcsA for $K^+$ can largely be explained thermodynamically: partitioning of the more strongly solvated $Na^+$ ions into the narrow pore is unfavourable[8–10], reflected in a difference between the free energy of $K^+$ and $Na^+$ in the pore and in the bulk solution

$$\Delta\Delta G(K^+ \rightarrow Na^+) = [(G_{pore}(Na^+) - G_{bulk}(Na^+)) - (G_{pore}(K^+) - G_{bulk}(K^+))] \quad (1)$$

that is larger than zero. Ion-flux measurements[11–13] indicate that the relative free energy of selectivity $\Delta\Delta G$ is of the order of 5–6 kcal mol$^{-1}$ for $K^+$ channels. This preference for $K^+$ ions is usually explained by pointing out that the channel can compensate for the desolvation of a cation of the correct radius like $K^+$ because it fits snugly into the narrow pore, whereas a sufficiently favourable interaction is not possible in the case of a smaller ion such as $Na^+$ (refs 1, 5, 7). This explanation is consistent with the observation that the selectivity filter in the X-ray structure of the KcsA channel is well adapted to coordinate $K^+$ (refs 5, 7). However, the atomic radii of $K^+$ and $Na^+$ differ only by 0.38 Å (ref. 14), so the snug-fit mechanism requires the selectivity filter to rigidly retain a precise (sub-ångstrom) geometry to discriminate between these two cations, even though proteins are 'soft materials' displaying significant structural flexibility[2,3,15]. The crystallographic thermal B-factors of the KcsA X-ray structure determined at 2.0 Å resolution are indicative of root-mean-square (r.m.s.) fluctuations of the order of about 0.75 Å (see also Supplementary Information)[7], in general accord with the structural fluctuations seen in molecular dynamics (MD) simulations of the KcsA channel[16–22]. The experimental observation that $K^+$ is needed for the overall stability of the channel structure[23,24] further supports the notion of a structurally flexible pore. In fact, the diameter of some regions of the pore in the X-ray structure is smaller than the size of $K^+$ (ref. 7), so flexibility and fluctuations seem to be essential for rapid conduction[19]. MD free-energy perturbation (FEP) computations help to elucidate the origin of energetic factors in dynamic structures[16–19], which in the case of a KcsA channel with full structural flexibility yielded ion selectivity in agreement with experimental estimates[11–13], despite atomic fluctuations of the order of ~1.0 Å r.m.s. (Fig. 1). Taken together, these observations indicate that a snug structural fit of $K^+$ inside the narrow and rigid pore is not the origin of the ion selectivity seen in potassium channels.

An alternative explanation is that selectivity might arise locally, from the intrinsic physical properties of the ligands coordinating the ions passing through the channel[25]. The most important local interactions are the very strong electrostatic attraction and core repulsion between the cation and the nearest carbonyl groups, and the moderate electrostatic repulsion between the coordinating carbonyl groups themselves. To probe their role in achieving ion selectivity, we monitor changes in $\Delta\Delta G$ upon artificially disrupting these interactions. The effect of turning off the electrostatic interaction between the carbonyls on $\Delta\Delta G$ is particularly informative because it is associated with the dynamical properties of the coordination shell (that is, $\Delta\Delta G$ should not be affected if the coordination structure is rigid). In the following, we compare and contrast the results from FEP computations with and without carbonyl electrostatic repulsion in the KcsA channel with those

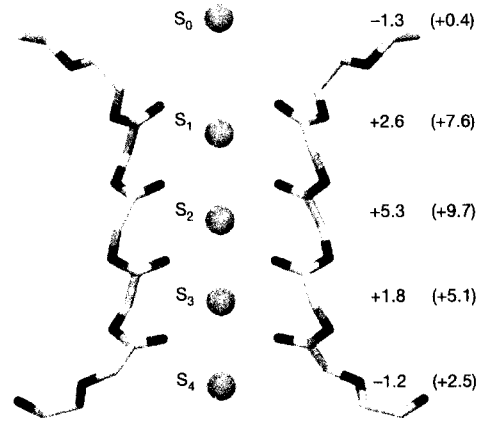


**Figure 1** Schematic structure of the cation binding sites in the selectivity filter of the KcsA channel[7]. Only two subunits are depicted for clarity. The extracellular side is on the top and the intracellular side is at the bottom. Results from both X-ray crystallography[7] and MD free-energy simulations[19] show that five specific cation binding sites ($S_0$ to $S_4$) are disposed along the narrow pore of the KcsA $K^+$ channel. The cation positions are represented (green) and the carbonyl oxygen group of residues Thr 75, Val 76, Gly 77 and Tyr 78 are shown explicitly (red). Computational studies show that ion movement through the channel takes place in a concerted way, as the $K^+$ in the pore undergo hopping transitions between stable multi-ion configurations: $[S_3, S_1] \leftrightarrow [S_4, S_2, S_0] \leftrightarrow [S_4, S_2] \leftrightarrow [S_3, S_1]$ (ref. 20), consistent with structural data[6,7]. Only configurations in which the cations are separated by one water molecule are allowed. The numbers adjacent to the binding sites are the $\Delta\Delta G$ (in kcal mol$^{-1}$) obtained from FEP computations based on the KcsA channel in a fully solvated lipid membrane (see Methods). Similar computations based on a frozen channel structure perfectly adapted to $K^+$ indicate that it is very selective (numbers in parentheses).

obtained in liquid N-methylacetamide (NMA), a generic model of the protein backbone, and valinomycin, a cationic membrane carrier exhibiting a very high selectivity for $K^+$ over $Na^+$ (refs 26, 27). The FEP calculations for the KcsA channel are focused on the site $S_2$, located near the middle of the narrow pore, which is the most selective (Fig. 1). The results are reported in Table 1.

Removing the carbonyl–carbonyl interaction in a fully flexible KcsA channel annihilates the selectivity of the site $S_2$, which then becomes favourable for $Na^+$. The relative free energy, originally unfavourable for $Na^+$ by 5.3 kcal mol$^{-1}$, becomes favourable by $-2.9$ kcal mol$^{-1}$ with a net loss of 8.2 kcal mol$^{-1}$ in selectivity when the repulsive interaction between the backbone carbonyl is turned off (Table 1). *Ab initio* computations on model systems indicate that non-additive electronic polarization (neglected in the present pair-wise all-atom force field)[28] would make the free-energy contribution arising from carbonyl–carbonyl repulsion even more unfavourable. Very strong positional energy restraints (30 kcal mol$^{-1}$ Å$^{-2}$) must be applied to the KcsA atoms to maintain a selectivity of about 5 to 6 kcal mol$^{-1}$ in the absence of the carbonyl–carbonyl repulsion, essentially freezing the channel. The magnitude of the free-energy change in liquid NMA (10.5 kcal mol$^{-1}$) is very similar to that found in the fully flexible KcsA channel, suggesting that the coordination of the ions in the selectivity filter of KcsA is indeed very dynamical and 'liquid-like'. Consistent with this view, the width of the main peak in the radial distribution between the cation and the surrounding oxygen ligands shown in Fig. 2 is similar for KcsA and liquid NMA (of the order of 1.0 Å).

To further assess the importance of protein rigidity relative to the local interactions, additional FEP calculations were performed, keeping all channel atoms fixed except those forming the selectivity filter (that is, the backbone atom of residues Thr 74 to Asp 78). In particular, the aromatic side chains suggested to play an essential role in the selectivity (that is, Tyr 78, Trp 67, Trp 68)[5] were kept frozen at their X-ray structure positions. Removing carbonyl repulsion in the selectivity filter results in a loss of almost 6 kcal mol$^{-1}$ of selectivity for $K^+$ over $Na^+$ (Table 1), despite the frozen protein surrounding the selectivity filter. Although most conserved residues are essential for the overall stability of the three-dimensional fold (within ~1 Å), the FEP calculations show that the architectural sub-ångstrom rigidity of the protein conferred by the residues surrounding the selectivity filter is not a key factor in making the channel selective for $K^+$ over $Na^+$.

Despite its large impact on the relative free energy of solvation of cations in the pore, the carbonyl–carbonyl ligand repulsion has a moderate influence on pore structure. On average, the repulsion between the eight carbonyl groups renders the system 14 kcal mol$^{-1}$ less stable when $Na^+$ occupies the $S_2$ site than when $K^+$ is present. This difference is much smaller than the large interaction energy between the cation and its surroundings (roughly $-150$ and $-170$ kcal mol$^{-1}$ for $K^+$ and $Na^+$, respectively). The local coordination structure is thus controlled by the strong ion–carbonyl interactions, with $K^+$ as well as $Na^+$ being well-coordinated in the flexible and fluctuating pore; see the radial distribution function between the central cation ($K^+$ or $Na^+$) and its coordinating oxygens (Fig. 2). In fact, the average structure is not strongly affected when removing the electrostatic repulsion between the carbonyl groups; for example, the coordination numbers with and without repulsion are quite similar (Fig. 2). The carbonyl–carbonyl repulsion thus has little effect on the pore radius, but instead influences ion-binding energetics. This is in accord with behaviour generally seen in flexible systems undergoing thermal fluctuations (for example, a liquid), where the harshest and strongest interactions dictate the average structure while weaker interactions modulate thermodynamics (for example, the core repulsion and London dispersion in a van der Waals liquid)[29].

The ion selectivity of valinomycin is higher than that of KcsA and liquid NMA, although the trends are qualitatively similar (Table 1). As indicated by the narrow width of the radial distribution function (Fig. 2), this cyclic ionophore is more rigid and less able to adapt to coordinate $Na^+$ than KcsA or liquid NMA as a result of its high covalent connectivity (only three chemical bonds separate each carbonyl group from its neighbours). $K^+$ is coordinated by six carbonyl oxygen atoms, whereas $Na^+$ is coordinated by only four carbonyl oxygens (Fig. 2), which increases ion selectivity. In contrast, the selectivity filter of KcsA and liquid NMA are more flexible

Table 1 **Importance of carbonyl–carbonyl repulsion on free energy**

| System | $\Delta\Delta G$ with all interactions (kcal mol$^{-1}$) | $\Delta\Delta G$ with no repulsion (kcal mol$^{-1}$) | Loss in ion selectivity (kcal mol$^{-1}$) |
|---|---|---|---|
| Fully flexible KcsA | 5.3 | −2.9 | 8.2 |
| Fully frozen KcsA | 9.7 | 9.7 | 0.0 |
| Restrained KcsA | 8.6 | 5.9 | 2.7 |
| Partly frozen KcsA | 6.7 | 0.9 | 5.8 |
| Liquid NMA | 1.6 | −8.9 | 10.5 |
| Valinomycin | 8.8 | 3.9 | 4.9 |

All calculations with KcsA concern exclusively the $S_2$ binding site and are based on the X-ray structure PDB id 1K4C. Fully flexible KcsA, all-atom MD/FEP with fully flexible KcsA embedded in DPPC membrane. Fully frozen KcsA, all-atom MD/FEP with KcsA embedded in DPPC membrane with all channel atoms frozen in the X-ray position. Restrained KcsA, all-atom MD/FEP with KcsA embedded in DPPC membrane with all non-hydrogen channel atoms submitted to a harmonic restraint of 30 kcal mol$^{-1}$ Å$^{-2}$ relative to the X-ray position, yielding RMS fluctuations of 0.11 Å for the backbone of the selectivity filter. Partly frozen KcsA, all-atom MD/FEP with KcsA embedded in DPPC membrane allowing motions only for the backbone atoms of the selectivity filter (residues Thr 74 to Asp 78), all other channel atoms are frozen in the X-ray position. Liquid NMA, relative solvation free energy between liquid water and liquid NMA. Valinomycin, relative free energy of ions bound to valinomycin solvated in ethanol.

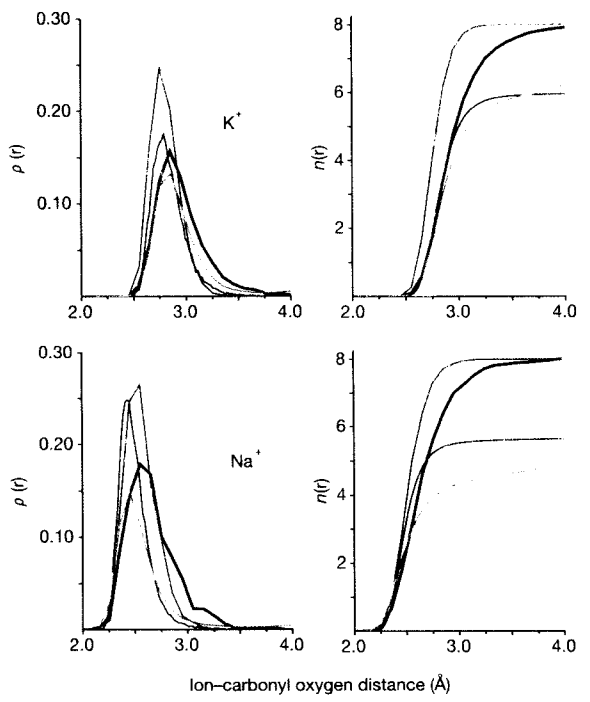


**Figure 2** Ion–carbonyl oxygen pair correlation function $\rho(r)$ and coordination number $n(r)$ in different environments. The results for the $S_2$ binding site of the KcsA selectivity filter with all interactions (solid black line) and without the carbonyl–carbonyl repulsion (solid red line) are shown for $K^+$ (top) and $Na^+$ (bottom). For comparison, the corresponding quantities are shown for the X-ray structure (dotted black line), liquid NMA (solid blue line) and in valinomycin (solid green line). The shift in the position of the maximum in the radial distribution for both ions in the selectivity filter of KcsA when carbonyl repulsion is excluded is less than 0.1 Å, much smaller than the width of the main peak (~1.0 Å). In comparison, the shift in the peak position is about 0.32 Å between $K^+$ and $Na^+$ when all interactions are included.

than valinomycin. In liquid NMA, $K^+$ and $Na^+$ are coordinated by six carbonyl oxygens whereas they are coordinated by six to eight oxygens in the binding site $S_2$ of KcsA. The coordination structure is liquid-like in both cases, but selectivity is more pronounced for the site $S_2$ of KcsA than for liquid NMA (see Supplementary Information). Further analysis with a simple model suggests that one mechanism for increasing selectivity in a flexible structure is to increase the number of coordinating ligands surrounding the cation (see below).

Although this is not the underlying mechanism of selectivity, the pore is nonetheless structurally well-adapted to coordinate $K^+$ with minimal structural strain. For example, the peak in the $K^+$–oxygen radial distribution function corresponds to the X-ray structure (Fig. 2). The adaptation of the protein surrounding the selectivity filter is perhaps best illustrated by considering the results of *ab initio* geometry optimization of $K^+$ in the central binding site $S_2$. Representing the four subunits forming the binding site as glycine dipeptides, the optimized *ab initio* geometry is seen to depart by 0.28 Å r.m.s. from the high-resolution X-ray structure of KscA. Such a relatively small deviation (in the absence of the rest of the protein) suggests that the channel has evolved to optimize the location and structure of the ligands coordinating $K^+$. But selectivity would be highly sensitive to the sub-ångstrom precision of the selectivity filter if such structural adaptation translated into structural rigidity: additional *ab initio* calculations show that deviation of the four subunits from the optimized configuration by a mere 0.15 Å would be sufficient to abolish the preference for $K^+$ if the structure were static. Remarkably, thermal fluctuations have the ability to protect the selectivity of the pore for $K^+$ against such minor structural changes. To illustrate this unexpected feature of a dynamical fluctuating pore, a reduced model limited to the cation-binding site $S_2$ was considered. This simple model, comprising only 37 atoms, is depicted in Fig. 3a (see legend for details). Similar FEP calculations were repeated, imposing restraints on the atoms of the model to control the magnitude of atom fluctuations in the system. The dependence of $\Delta\Delta G$ on the magnitude of the allowed r.m.s. atomic fluctuations is plotted in Fig. 3b. As expected, the free energies of selectivity are quite similar with and without carbonyl repulsions if atomic fluctuations smaller than 0.1 Å are permitted. But when the repulsion between the carbonyls is removed, the site becomes progressively more selective for $Na^+$ as the flexibility of the model increases. To ascertain the importance of the geometry of the binding site, FEP calculations were repeated using a model of $S_2$ optimized for coordinating $Na^+$ as a reference structure. As shown in Fig. 3b, this binding site is very favourable for $Na^+$ as long as the system is kept rigid and only atomic fluctuations smaller than 0.3 Å are allowed. But this enforced binding preference is destroyed as thermal fluctuations become larger, with selectivity for $K^+$ over $Na^+$ restored as thermal fluctuations of ~0.7 Å are allowed, effectively 'rescuing' the intrinsic binding propensity of the site. Selectivity is thus clearly a robust feature by virtue of the flexible and fluctuating

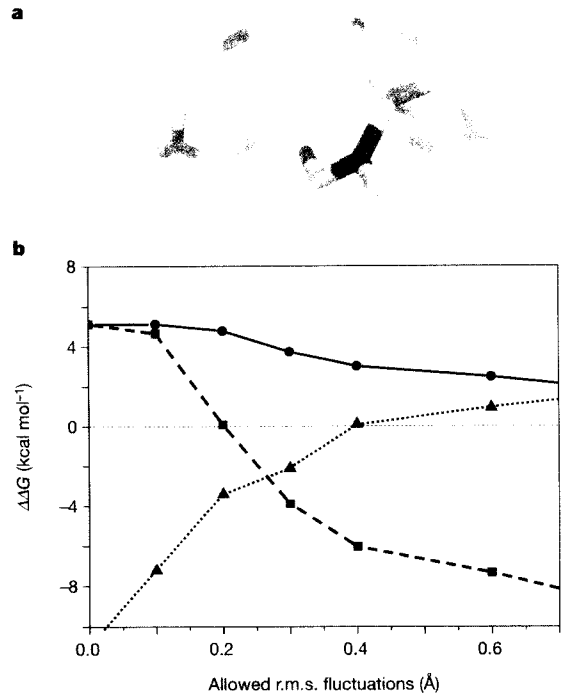


**Figure 3** Selectivity of a model of the KcsA binding site $S_2$ as a function of flexibility. **a**, The structure of the model used to mimic the site $S_2$ is shown. **b**, The results of the FEP calculations using the X-ray structure of KcsA[7] as a reference with all interactions (solid line with circles) and excluding the carbonyl–carbonyl repulsion (dashed line with squares) are shown. The results of the FEP calculations using a reference structure optimized to best-coordinate a smaller cation such as $Na^+$ ion in the binding site (obtained via energy minimization in vacuum) are also shown (dotted line with triangles). In all cases, the maximum r.m.s. fluctuations were controlled using a flat-bottomed steep harmonic potential imposed on all the non-hydrogen protein atoms of the model.

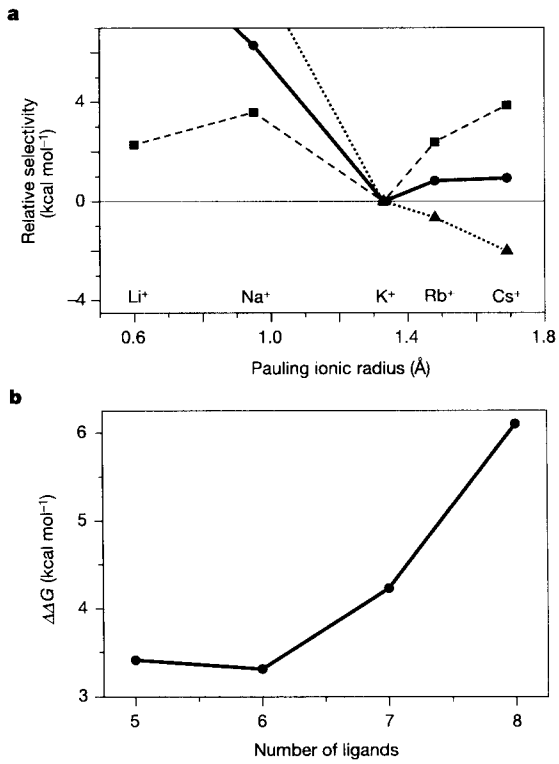


**Figure 4** Intrinsic selectivity of a simple model of freely fluctuating carbonyl-like dipoles. **a**, The variations of $\Delta\Delta G$ as a function of ionic radius are shown. The calculations are based on the FEP computations done on a simple model of one cation surrounded by eight carbonyl-like dipoles (comprising two atoms) with the oxygen atoms allowed to move freely within a sphere of radius 3.5 Å. Different cases are illustrated: cation surrounded by eight dipoles of 3.0 debye (solid black line with circles); eight dipoles of 4.2 debye (dashed line with squares) and eight dipoles of 1.8 debye (dotted line with triangles). The results of the FEP calculations for the five cations are plotted using standard ionic radii[14] (the $\Delta\Delta G$ values for the different cases were shifted to bring $K^+$ to zero). **b**, The dependence of $\Delta\Delta G$ on the number of surrounding carbonyl-like dipoles is illustrated. The selectivity is strongly influenced by the number of carbonyl–carbonyl repulsive pairs (that is, $n(n-1)/2$ for $n$ carbonyl groups).

nature of the system, with carbonyl–carbonyl repulsion ensuring the system's selectivity for $K^+$ binding.

The present analysis shows that ionic selectivity in $K^+$ channels is primarily determined by the intrinsic physical properties of the ligands coordinating the cation in the binding site, rather than by the precise sub-ångstrom geometry of the carbonyl oxygens lining a rigid pore. While this perspective contrasts sharply with structure-based views of ionic selectivity in $K^+$ channels[1,5–7], it shares some of the underlying principles of treatments that identify the strength of the electric field arising from the ligands coordinating the cation in a binding site as a key factor in determining selectivity[4]. In this context, we assess the magnitude of the ligand dipoles required to maintain a robust ionic selectivity in a flexible system undergoing thermal fluctuations. We consider a simple model with eight carbonyl-like (C = O) dipoles surrounding a central cation fluctuating freely inside a sphere of 3.5 Å radius. The FEP calculations depicted in Fig. 4 (see legend for details) reveal that such a simple system is naturally selective for $K^+$ if the ligand dipoles have a magnitude of about 3 debye, a value that is very close to the dipole moment of the protein backbone carbonyl group[28]. This result further demonstrates that significant selectivity for $K^+$ over $Na^+$ is possible without any need for architectural rigidity that would prevent the coordinating ligands from collapsing onto a smaller cation.

The main findings from the simple model are consistent with the existence of the conserved TTVGYG motif, which is structurally needed to fold the polypeptide chain into the ion-conducting conformation with the main-chain carbonyl oxygens oriented towards a central pore axis[5]. The selectivity displayed by the simple model is sensitive to the number of coordinating groups; significant selectivity for $K^+$ over $Na^+$ is obtained only when eight freely fluctuating carbonyl-like dipoles are present (Fig. 4b). This explains the origin of the low $K^+$ selectivity in liquid NMA with six nearest neighbours in the first solvation shell (Fig. 2). It also suggests that the three-dimensional fold of the selectivity filter (Fig. 1) might serve to enhance the local 'concentration' of fluctuating carbonyl groups within a small region. The simple model with freely fluctuating carbonyl dipoles leaves out any factors related to protein geometry and rigidity, yet displays qualitative trends in good accord with experimental observations: the selectivity for $K^+$ over $Na^+$ is of the order of 5–6 kcal $mol^{-1}$, whereas the selectivity over $Rb^+$ and $Cs^+$ is somewhat smaller[9,10]. The flexible binding site remains optimal for $K^+$ as long as the coordinating ligands have a dipole roughly between 2.5 and 4.5 debye, that is, are carbonyl-like. Increasing the magnitude of the dipoles beyond 4.5 debye favours smaller cations, whereas decreasing the dipoles has the opposite effect (Fig. 4a). However, decreasing the magnitude of only four out of eight carbonyl dipoles does not alter the selectivity significantly, in accord with experiments introducing a backbone ester carbonyl mutation in the selectivity filter[30]. These observations are consistent with the classical concept of 'field strength' developed by Eisenman[4], although the present analysis incorporates also the influence of thermal atomic fluctuations and ligand–ligand repulsion.

A sharp departure from eight identical carbonyl-like fluctuating ligands is required to make the site favourable for $Na^+$ over $K^+$; for example, it becomes selective for $Na^+$ when the magnitude of the dipoles is ~7 debye. One possible way of achieving $Na^+$ selectivity (although there are others) would be the introduction of charged residues forming a salt bridge directly into the pore. It is intriguing that the amino acids identified to be essential for the selectivity of Na-channels include the highly conserved DEKA locus from four different protein domains[10,31]. Selectivity for $K^+$ or for $Na^+$ clearly requires different chemical functionalities to coordinate the cation favourably, in accord with the observation that no biological channels selective to $Na^+$ appear to have evolved by refining the geometry of a KcsA-like pore lined by backbone carbonyl groups[10]. □

## Methods

### Models

The atomic system and simulation methodology have been described elsewhere[7]. Briefly, the total number of atoms in protein simulations is slightly above 40,000 (KcsA, 112 dipalmitoyl phosphatidylcholine, 6,778 water molecules, three $K^+$ ions in the pore, six $K^+$ and 21 $Cl^-$ ions in the bulk solutions). The high-resolution structure of the channel was used[7]. The X-ray coordinates were relaxed by less than 0.12 Å to remove any strain in the reference structure. The simple model system for the $S_2$ binding site occupied by a $K^+$ (37 atoms with one cation) was taken directly from this structure (Fig. 3a). The corresponding model system for the $S_2$ binding site occupied by a $Na^+$ was refined by energy minization in vacuum to generate an optimal coordination for this cation; the resulting structure retained the overall four-fold symmetry but was slightly collapsed onto the smaller cation, deviating from the original structure with $K^+$ by about 0.51 Å. Two different starting configurations of KcsA embedded in a solvated lipid membrane ('$S_0S_2S_2S_1$' and '$S_2S_2$cavity') were prepared using the previously published protocols[7]. The FEP computations on the binding sites of KcsA were carried using those configurations, alchemically transforming one cation at a time. FEP simulations of ion solvation in liquid NMA were carried out using a cubic box of 150 NMA molecules and one ion. FEP simulations of ion selectivity in valinomycin were carried out using a cubic box of 225 ethanol molecules. See Supplementary Information for more detail about the NMA and valinomycin systems.

### Computational procedure

All MD simulations and FEP computations were carried out using a modified version of the program CHARMM[32]. The total length of simulation preceding the FEP computations was over 1.8 ns. The resulting structure was used to perform the FEP calculations in each binding sites (Fig. 1). The variation in $\Delta\Delta G$ along the pore is associated with the hydration of the cation in the different binding sites (Fig. 1); similar results[19] were obtained using the X-ray structure at lower resolution[5]. The binding sites $S_1$ and $S_3$ near the ends of the selectivity filter are less selective (cations in those sites are not completely dehydrated, but maintain some contacts with one or two water molecules) whereas a cation in $S_2$ is completely dehydrated and coordinated by eight backbone carbonyl oxygens (from Gly 77 and Val 76). To remove the carbonyl–carbonyl repulsion, the Coulomb interactions between those atoms were simply skipped from the main loop in the total energy and forces calculation (this procedure differs from a direct scaling of the partial charges of the carbonyl to zero, because all the electrostatic interactions of the carbonyl with the ions, water molecules and with the remainder of the system remain unaffected). The selectivity filter simulated with and without carbonyl repulsion deviate only by 0.5 Å from one another (the average r.m.s. relative to the X-ray structure is 0.7 Å with repulsion and 0.6 Å without repulsion).

For each of the FEP computation (KcsA, valinomycin, liquid NMA, and the simple models used in Figs 3 and 4), the forward and backward directions free-energy perturbation ($K^+ \rightarrow Na^+$) had values of coupling parameter λ varying from 0 to 1 by increments of 0.05 for a total 1.1 ns. All calculations with the frozen or restrained channel structure were carried out according to the same FEP protocol (except that all or some channel atoms are kept fixed at all times) as described previously[19]. The potential function of the ions was parameterized to yield an accurate description of solvation in bulk water and liquid amides. The Lennard–Jones parameters for cations were adjusted to reproduce the experimental free energies of solvation as described previously[19]. Solvation free energies in water were calculated using FEP. For the rest of the atoms, the standard PARAM-22 force field was used[33]. To assess the importance of non-additive forces associated with induced electronic polarization on the FEP computations, *ab initio* computations were performed for a model system of two NMA molecules coordinating one cation ($K^+$ or $Na^+$; the results are given in the Supplementary Information).

Received 28 April; accepted 17 August 2004; doi:10.1038/nature02943.


1. Hille, B., Armstrong, C. M. & MacKinnon, R. Ion channels: From idea to reality. *Nature Med.* **5,** 1105–1109 (1999).
2. Zaccai, G. How soft is a protein? A protein dynamics force constant measured by neutron scattering. *Science* **288,** 1604–1609 (2000).
3. Karplus, M. & Petsko, G. A. Molecular dynamics simulations in biology. *Nature* **347,** 631–639 (1990).
4. Eisenman, G. Cation selective electrodes and their mode of operation. *Biophys. J.* **2,** 259–323 (1962).
5. Doyle, D. A. *et al.* The structure of the potassium channel: molecular basis of $K^+$ conduction and selectivity. *Science* **280,** 69–77 (1998).
6. Morais Cabral, J. H., Zhou, Y. F. & MacKinnon, R. Energetic optimization of ion conduction rate by the $K^+$ selectivity filter. *Nature* **414,** 37–42 (2001).
7. Zhou, Y., Morais Cabral, J. H., Kaufman, A. & MacKinnon, R. Chemistry of ion coordination and hydration revealed by a $K^+$ channel-Fab complex at 2.0 Å resolution. *Nature* **414,** 43–48 (2001).
8. Eisenman, G. & Horn, R. Ion selectivity revisited: the role of kinetic and equilibrium processes in ion permeation through channels. *J. Membr. Biol.* **76,** 197–225 (1983).
9. Latorre, R. & Miller, C. Conduction and selectivity in potassium channels. *J. Membr. Biol.* **71,** 11–30 (1983).
10. Hille, B. *Ion Channels of Excitable Membranes* 3rd edn (Sinauer, Sunderland, Massachusetts, 2001).
11. Neyton, J. & Miller, C. Discrete $Ba^{2+}$ block as a probe of ion occupancy and pore structure in the high conductance $Ca^{2+}$ activated $K^+$ channel. *J. Gen. Physiol.* **92,** 569–596 (1988).
12. LeMasurier, M., Heginbotham, L. & Miller, C. KcsA: it's a potassium channel. *J. Gen. Physiol.* **118,** 303–314 (2001).
13. Nimigean, C. M. & Miller, C. $Na^+$ block and permeation in $K^+$ channel of known structure. *J. Gen. Physiol.* **120,** 323–325 (2002).
14. Pauling, L. *Nature of the Chemical Bond and Structure of Molecules and Crystals* 3rd edn (Cornell Univ. Press, Ithaca, 1960).
15. Allen, T. W., Andersen, O. S. & Roux, B. On the importance of atomic fluctuations, protein flexibility

and solvent in ion permeation. *J. Gen. Physiol.* (in the press).
16. Åqvist, J. & Luzhkov, V. Ion permeation mechanism of the potassium channel. *Nature* **404,** 881–884 (2000).
17. Luzhkov, V. B. & Aqvist, J. $K^+/Na^+$ selectivity of the KcsA potassium channel from microscopic free energy perturbation calculations. *Biochim. Biophys. Acta* **1548,** 194–202 (2001).
18. Allen, T. W., Bliznyuk, A., Rendell, A. P., Kuyucak, S. & Chung, S. H. The potassium channel: Structure, selectivity and diffusion. *J. Chem. Phys.* **112,** 8191–8204 (2000).
19. Berneche, S. & Roux, B. Energetics of ion conduction through the $K^+$ channel. *Nature* **414,** 73–77 (2001).
20. Berneche, S. & Roux, B. A microscopic view of ion conduction through the $K^+$ channel. *Proc. Natl Acad. Sci. USA* **100,** 8644–8648 (2003).
21. Shrivastava, I. H., Tieleman, D. P., Biggin, P. C. & Sansom, M. S. P. $K^+$ versus $Na^+$ ions in a K channel selectivity filter: A simulation study. *Biophys. J.* **83,** 633–645 (2002).
22. Guidoni, L., Torre, V. & Carloni, P. Potassium and sodium binding to the outer mouth of the $K^+$ channel. *Biochemistry* **38,** 8599–8604 (1999).
23. Doboda, A., Melishchuk, A. & Armstrong, C. Dilated and defunct K channels in the absence of $K^+$. *Biophys. J.* **80,** 2704–2714 (2001).
24. Zhou, Y. F. & MacKinnon, R. The occupancy of ions in the $K^+$ selectivity filter: Charge balance and coupling of ion binding to a protein conformational change underlie high conduction rates. *J. Mol. Biol.* **333,** 965–975 (2003).
25. Yamashita, M. M., Wesson, L., Eisenman, G. & Eisenberg, D. Where metal ions bind in proteins. *Proc. Natl Acad. Sci. USA* **87,** 5648–5652 (1990).
26. Aqvist, J., Alvarez, O. & Eisenman, G. Ion-selective properties of a small ionophore in methanol studied by free energy perturbation simulations. *J. Phys. Chem.* **96,** 10019–10025 (1992).
27. Marrone, T. J. & Merz, K. M. Jr. Molecular recognition of $K^+$ and $Na^+$ by valinomycin in methanol. *J. Am. Chem. Soc.* **117,** 779–791 (1995).
28. MacKerell, A. D. J. *et al.* All-atom empirical potential for molecular modeling and dynamics studies of proteins. *J. Phys. Chem. B* **102,** 3586–3616 (1998).
29. Weeks, J. D., Chandler, D. & Andersen, H. C. Role of repulsive forces in determining the equilibrium structure of simple liquids. *J. Chem. Phys.* **54,** 5237–5247 (1971).
30. Lu, T. *et al.* Probing ion permeation and gating in a $K^+$ channel with backbone mutations in the selectivity filter. *Nature Neurosci.* **4,** 239–246 (2001).
31. Heinemann, S. H., Terlau, H., Stuhmer, W., Imoto, K. & Numa, S. Calcium channel characteristics conferred on the sodium channel by single mutations. *Nature* **356,** 441–443 (1992).
32. Brooks, B. R. *et al.* CHARMM: a program for macromolecular energy minimization and dynamics calculations. *J. Comput. Chem.* **4,** 187–217 (1983).

**Supplementary Information** accompanies the paper on **www.nature.com/nature**.

**Acknowledgements** Discussions with G. Eisenman, J. Aqvist, O. Andersen, C. Miller and D. Doyle are gratefully acknowledged. This work was funded by the NIH and by the American Epilepsy Society and UCB Pharma Inc. to S.Yu.N. This work was supported by the National Center for Supercomputing Applications (NCSA) at the University of Illinois, Urbana-Champaign, the Pittsburgh Supercomputing Center (PSC), and the Scientific Computing and Visualization (SCV) group at Boston University.

**Competing interests statement** The authors declare that they have no competing financial interests.

**Correspondence** and requests for materials should be addressed to B.R. (benoit.roux@med.cornell.edu)

# Low marine sulphate and protracted oxygenation of the Proterozoic biosphere

**Linda C. Kah[1], Timothy W. Lyons[2] & Tracy D. Frank[3]**

[1]*Department of Earth and Planetary Sciences, University of Tennessee, Knoxville, Tennessee 37996, USA*
[2]*Department of Geological Sciences, University of Missouri, Columbia, Missouri 65211, USA*
[3]*Department of Geosciences, University of Nebraska, Lincoln, Nebraska 68588, USA*

**Progressive oxygenation of the Earth's early biosphere is thought to have resulted in increased sulphide oxidation during continental weathering, leading to a corresponding increase in marine sulphate concentration[1]. Accurate reconstruction of marine sulphate reservoir size is therefore important for interpreting the oxygenation history of early Earth environments. Few data, however, specifically constrain how sulphate concentrations may have changed during the Proterozoic era (2.5–0.54 Gyr ago). Prior to 2.2 Gyr ago, when oxygen began to accumulate in the Earth's atmosphere[2,3], sulphate concentrations are inferred to have been <1 mM and possibly <200 μM, on the basis of limited isotopic variability preserved in sedimentary sulphides[4] and experimental data showing suppressed isotopic fractionation at extremely low sulphate concentrations[1,5]. By 0.8 Gyr ago, oxygen and thus sulphate levels may have risen significantly[6,7]. Here we report large stratigraphic variations in the sulphur isotope composition of marine carbonate-associated sulphate, and use a rate-dependent model for sulphur isotope change that allows us to track changes in marine sulphate concentrations throughout the Proterozoic. Our calculations indicate sulphate levels between 1.5 and 4.5 mM, or 5–15 per cent of modern values, for more than 1 Gyr after initial oxygenation of the Earth's biosphere. Persistence of low oceanic sulphate demonstrates the protracted nature of Earth's oxygenation. It links biospheric evolution to temporal patterns in the depositional behaviour of marine iron- and sulphur-bearing minerals[4], biological cycling of redox-sensitive elements[6] and availability of trace metals essential to eukaryotic development[8].**

To understand Proterozoic biospheric oxygenation better, we have modified an existing model for C isotope variability[9] to estimate marine sulphate reservoir size using rates of S isotope variation. These rates are recorded stratigraphically as variation in the S isotope composition of evaporitic gypsum and carbonate-associated sulphate (CAS). Because CAS is routinely trapped in marine carbonates[10] and, in organic-poor sediments, is isotopically buffered against appreciable diagenetic overprints[11], it can record the $\delta^{34}S$ signal of marine sea water even when gypsum is lacking. Furthermore, CAS is a more direct proxy for marine sea water than sedimentary pyrite, the isotopic composition of which is complicated by local reservoir effects and varying fractionations during bacterial sulphate reduction (BSR)[12].

In our model, the isotopic composition of marine sulphate changes in response to imbalances in isotopic fluxes into and out of a non-steady state system (see Methods). In the modern ocean, sulphate concentrations of 28.4 mM effectively buffer the isotopic system from changing at rates exceeding 0.5‰ per Myr, despite large fractionations associated with the modern bacterial sulphur cycle (Fig. 1). Long-term variation in the isotopic composition of

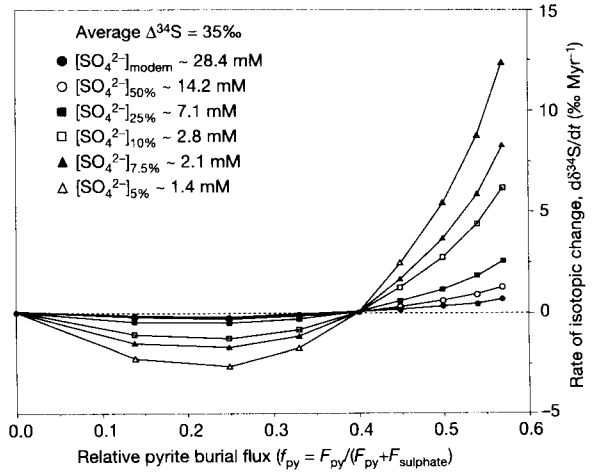


**Figure 1** Sensitivity of the marine sulphate system to reservoir size. At average fractionations observed within the modern bacterial sulphur cycle ($\Delta S = 35‰$), modern reservoir sizes effectively buffer the marine system from the large S isotope shifts that characterize Proterozoic stratigraphic sections, even at moderate to high degrees of pyrite burial ($f_{py} = 0.2–0.6$).